The Journal of Physiology

Synaptic communication within the microcircuits of pyramidal neurons and basket cells in the mouse prefrontal cortex

Zsuzsanna Fekete[1,2], Filippo Weisz[1], Mária Rita Karlócai[1], Judit M. Veres[1], Tibor Andrási[1] and Norbert Hájos[1,3,4]

[1] *Institute of Experimental Medicine, Budapest, Hungary*
[2] *János Szentágothai School of Neurosciences, Semmelweis University, Budapest, Hungary*
[3] *The Linda and Jack Gill Center for Molecular Bioscience, Indiana University Bloomington, Indiana, USA*
[4] *Program in Neuroscience, Department of Psychological and Brain Sciences, Indiana University Bloomington, Indiana, USA*

Handling Editors: Katalin Toth & Jean-Claude Béïque

The peer review history is available in the Supporting Information section of this article (https://doi.org/10.1113/JP286284#support-information-section).

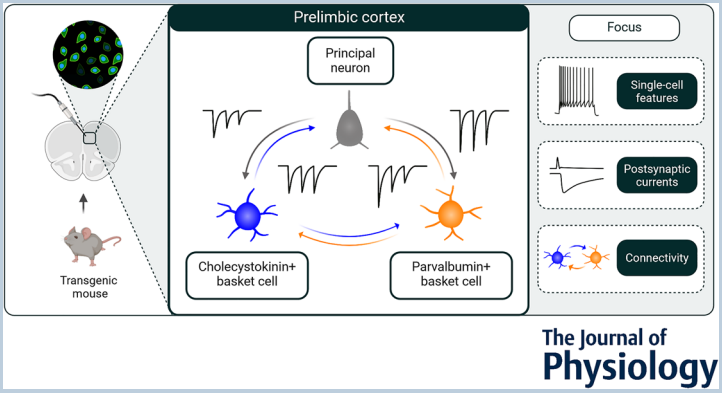

Abstract figure legend Basket cells represent critical building blocks of neuronal circuits in cortical regions by providing GABAergic innervation to the perisomatic region of their postsynaptic partners. In the mouse prelimbic cortex, the two basket cell types expressing parvalbumin or cholecystokinin/type I cannabinoid receptor receive unitary excitatory postsynaptic currents from local principal neurons with contrasting amplitude and latency. Basket cells also give rise to unitary inhibitory postsynaptic currents on principal cells that differ in terms of their reliability, latency and short-term plasticity. Moreover, the two basket cell types innervate each other in this cortical area. These fundamental features of the synaptic communication within the microcircuitry composed of pyramidal cells and two types of basket cells in the prelimbic cortex are critical for local information processing underlying complex network operation.

Zsuzsanna Fekete is a PhD candidate in neuroscience at the Semmelweis University Doctoral School, Budapest, Hungary. She obtained her BSc degree in biology and her MSc in cognitive science. Her research focuses on synaptic connections and circuit motifs with an interest in understanding the building blocks of neuronal circuit operations.

This article was first published as a preprint. Fekete Z, Weisz F, Karlócai MR, Veres JM, Andrási T, Hájos N. 2024. Synaptic communication within the microcircuits of pyramidal neurons and basket cells in the mouse prefrontal cortex. bioRxiv. https://doi.org/10.1101/2024.01.16.575904

DOI: 10.1113/JP286284

Abstract Basket cells are inhibitory interneurons in cortical structures with the potential to efficiently control the activity of their postsynaptic partners. Although their contribution to higher order cognitive functions associated with the medial prefrontal cortex (mPFC) relies on the characteristics of their synaptic connections, the way that they are embedded into local circuits is still not fully uncovered. Here, we determined the synaptic properties of excitatory and inhibitory connections between pyramidal neurons (PNs), cholecystokinin-containing basket cells (CCKBCs) and parvalbumin-containing basket cells (PVBCs) in the mouse mPFC. By performing paired recordings, we revealed that PVBCs receive larger unitary excitatory postsynaptic currents from PNs with shorter latency and faster kinetic properties compared to events evoked in CCKBCs. Also, unitary inhibitory postsynaptic currents in PNs were more reliably evoked by PVBCs than by CCKBCs, yet the former connections showed profound short-term depression. Moreover, we demonstrated that CCKBCs and PVBCs in the mPFC are connected with each other. Because alterations in PVBC function have been linked to neurological and psychiatric conditions such as Alzheimer's disease and schizophrenia and CCKBC vulnerability might play a role in mood disorders, a deeper understanding of the general features of basket cell synapses could serve as a reference point for future investigations with therapeutic objectives.

(Received 16 January 2024; accepted after revision 6 September 2024; first published online 18 October 2024)
Corresponding author N. Hájos: Institute of Experimental Medicine, Budapest 1083, Hungary. Email: nhajos@iu.edu

Key points

- Cholecystokinin- (CCKBCs) and parvalbumin-expressing basket cells (PVBCs) have distinct passive and active membrane properties.
- Pyramidal neurons give rise to larger unitary excitatory postsynaptic currents in PVBCs compared to events in CCKBCs.
- Unitary inhibitory postsynaptic currents in pyramidal neurons are more reliably evoked by PVBCs than by CCKBCs.
- Basket cells form chemical synapses and gap junctions with their own cell type.
- The two basket cell types are connected with each other.

Introduction

In the past decades, substantial effort has been made to associate different inhibitory cell types in cortical areas with specific functions in animal behaviour. Research on parvalbumin-containing basket cells (PVBCs), a GABAergic cell type frequently studied in cortical structures is a great example of these efforts. The role of PVBCs has been demonstrated in generating oscillations (Gulyas et al., 2010; Schlingloff et al., 2014; Sohal et al., 2009; Stark et al., 2014), working memory (Kim et al., 2016; Lagler et al., 2016) and sensory processing (Atallah et al., 2012; Bienvenu et al., 2012; Cardin et al., 2009). Knowledge regarding the function of the other basket cell type, the cholecystokinin-expressing basket cell (CCKBC), on the other hand, remains limited, although, as a result of their preference for innervating the perisomatic region of postsynaptic partners (Armstrong & Soltesz 2012; Freund & Katona 2007; Veres et al., 2017), both BC types are able to efficiently control the spiking of their targets (Cobb et al., 1995; Miles et al. 1996; Stark et al., 2014; Veres et al., 2017; Woodruff & Sah 2007). In a recent study, we determined that ∼50% of CCKBC and PVBC axon terminals in the mouse prelimbic cortex (PrL) formed close appositions with the somata and proximal dendrites of neurons (Nagy-Pal et al., 2023), which typifies basket cells in cortical areas (Gulyas et al., 1993; Halasy et al., 1996; Kubota et al., 2015; Somogyi et al., 1983; Veres et al., 2017). The similarity in the target distribution might endow the two BC types with comparable significance within the balanced communication of pyramidal neurons (PNs) and inhibitory cells.

Despite the similarity of the targeted subcellular regions, the two BC types differ in several single-cell level features. PVBCs are equipped with voltage-gated Na^+ channels showing fast inactivation alongside voltage-gated K^+ channels, including Kv3.1 and Kv3.2 channels ensuring high-frequency firing (Hu et al.,

2018; Rudy & McBain 2001). Additionally, P/Q-type voltage-gated Ca^{2+} channels enable precisely timed transmitter release from PVBC terminals (Glickfeld & Scanziani 2006; Hefft & Jonas 2005; Hu et al., 2014; Rudy & McBain 2001). CCKBCs, on the other hand, according to data from other cortical regions such as the hippocampus and amygdala, display regular spiking phenotype (Barsy et al., 2017; Daw et al., 2009; Glickfeld & Scanziani 2006; Szabo et al., 2010), are capable of asynchronous release (Daw et al., 2009; Hefft & Jonas 2005; Szabo et al., 2010) and express type I cannabinoid receptor (CB1) on their terminals (Hajos et al., 2000; Katona et al., 1999) through which their output is suppressed by signalling molecules released retrogradely from the postsynaptic PNs (Wilson & Nicoll 2001; Wilson et al., 2001). Data regarding PVBC properties in the medial prefrontal cortex (mPFC) are in line with these findings (Miyamae et al., 2017), although the CCKBC features are yet to be determined.

The synaptic connectivity of the two BC types was also described as vastly different. In the hippocampus and amygdala, PVBCs were found to evoke IPSCs in local PNs with shorter latency and faster kinetics than CCKBCs (Barsy et al., 2017; Hefft & Jonas 2005), whereas the amplitudes of these currents were described as comparable to (Daw et al., 2009; Glickfeld & Scanziani 2006; Veres et al., 2017) or larger (Szabo et al., 2010) than those evoked by CCKBC firing. CCKBCs, on the other hand, receive smaller excitatory currents from local PNs than the PVBCs do (Andrasi et al., 2017; Glickfeld & Scanziani 2006). Although representing a major excitatory input to BCs (Ahrlund-Richter et al., 2019; Hafner et al., 2019), these connections have not yet been characterized in association cortices such as the mPFC.

Data linking altered PV interneuron function with neuropsychiatric disorders such as schizophrenia (Glausier et al., 2014; Gonzalez-Burgos et al., 2015; Hashimoto et al., 2003) or Alzheimer's disease (Hijazi et al., 2023; Shu et al., 2023) demonstrate how important the contribution of BCs is to healthy network operations. These findings also highlight the therapeutic potential of specifically targeting BC operation, a goal that may be fostered by thorough understanding of the synaptic interactions of BCs within the mPFC microcircuits. Therefore, in the present study, we set out to reveal the characteristics of synaptic transmission between PNs and BCs in the PrL and to address the question whether the PrL is built up with synaptically interconnected populations of the two classes of BCs. Using *in vitro* whole-cell, patch clamp recordings, we revealed the single-cell properties of identified BCs and the characteristics of excitatory and inhibitory synaptic transmission between PNs and BCs, as well as functional synaptic connections between the two BC types supported by anatomical data.

Methods

Ethical approval

All procedures involving animals were performed according to methods approved by the Hungarian legislation (1998. XXVIII. section 243/1998, renewed in 40/2013) and approved by the Committee of the Scientific Ethics of Animal Research (22.1/360/3/2016 and PE/EA/218-7/2021). All procedures were conducted in compliance with the European convention for the protection of vertebrate animals used for experimental and other scientific purposes (Directive: 2010/63/EU). Every effort was taken to minimize animal suffering and the number of animals used. The authors understand the ethical principles under which *The Journal of Physiology* operates and confirm that this work complies with the journal's policy and regulations on animal experimentation (Grundy, 2015).

Animals

For this study, both male and female adult mice (median age = 79 days, Q1–Q3: 72–98 days) were used in the electrophysiological experiments from the following transgenic mouse strains: BAC-CCK-DsRed on a FVB/N background ($n = 35$) (Mate et al., 2013), BAC-PV-eGFP on a FVB/AntFx background ($n = 35$) (Meyer et al., 2002) and Pvalb-IRES-Cre (#01 7320; http://www.jax.org) on a C57Bl6 background crossed with BAC-CCK-DsRed ($n = 3$). For anatomical quantification, C57Bl6 ($n = 3$) and VGAT-IRES-Cre::BAC-CCK-GFP-coIN ($n = 4$) (Vereczki et al., 2021) adult [postnatal day (P)49–150] mice were used. The latter mice were generated by crossing VGAT-IRES-Cre (#01 9962; http://www.jax.org) on a C57Bl6 background and BAC-CCK-GFP-coIN on a FVB/N background. All mice were bred in the Medical Genetechnology Unit at the HUN-REN Institute of Experimental Medicine (Budapest, Hungary) and their offspring were used in the experiments. Animals were group housed and had access to food and water *ad libitum*.

Experimental design

Slice preparations. Animals were decapitated following deep anesthesia induced by isoflurane (4–5%) and the brain was quickly removed from the skull and was placed into an ice-cold solution containing (in mM) 252 sucrose, 2.5 KCl, 26 $NaHCO_3$, 0.5 $CaCl_2$, 5 $MgCl_2$, 1.25 NaH_2PO_4 and 10 glucose, bubbled with 95% O_2/5% CO_2 (carbogen gas). Next, 200 µm thick coronal slices were prepared with a vibratome (VT1200S; Leica Microsystems, Wetzlar, Germany) and were incubated in an interface-type holding chamber for at least 1 h in ACSF that contained (in mM): 126 NaCl, 2.5 KCl, 1.25 NaH_2PO_4,

2 $MgCl_2$, 2 $CaCl_2$, 26 $NaHCO_3$ and 10 glucose, bubbled with carbogen gas, and was let to gradually cool down from 36°C to room temperature.

Electrophysiology. For the recordings, slices were placed into a submerged-type of chamber and were perfused with ACSF maintained at 32°C with a flow rate of 1.5–2 mL min^{-1}. Patch clamp recordings were performed under visual guidance of a differential interference contrast microscope (FN-1; Nikon, Tokyo, Japan; or BX61W Olympus, Tokyo, Japan) using a 40× water dipping objective. Neurons were visualized with an sCMOS camera (Andor Technology, Belfast, UK) and fluorescent protein expression was tested with the aid of a mercury arc lamp. Patch pipettes (5–7 MΩ) were pulled with a PC-10 puller (Narishige, Tokyo, Japan) from borosilicate capillaries with an inner filament (thin-walled, outer diameter 1.5). Pipettes used for patching interneurons for paired recordings with PNs were filled with an intracellular solution containing (in mM): 110 K-gluconate, 4 NaCl, 2 Mg-ATP, 20 HEPES, 0.1 EGTA, 0.3 GTP (sodium salt) and 10 phosphocreatine, adjusted to pH 7.3 using KOH with an osmolarity of 290 mosmol L^{-1}, whereas 10 mM GABA and 0.2% biocytin were added on the day of the experiments. The intracellular solution used for recording PNs contained (in mM): 54 K-gluconate, 4 NaCl, 56 KCl, 2 Mg-ATP, 20 HEPES, 0.1 EGTA, 0.3 GTP (sodium salt) and 10 phosphocreatine adjusted to pH 7.3 using KOH, with an osmolarity of 290 mosmol L^{-1}. This latter solution was used with an additional 0.2% biocytin and 10 mM GABA when paired recordings were performed between two interneurons. For optogenetic and pharmacological experiments the following intracellular solution was used (in mM): 60 Cs-gluconate, 80 CsCl, 1 $MgCl_2$, 2 Mg-ATP, 10 HEPES, 3 NaCl and 5 QX-314-Cl adjusted to pH 7.4 using HCl with an osmolarity of 280 mosmol L^{-1} and 0.2% biocytin was added on the day of the experiments.

Whole-cell, patch clamp recordings were performed with a Multiclamp 700B amplifier (Molecular Devices, San Jose, CA, USA), low-pass filtered at 3 kHz and digitized at 10 kHz for recording firing patterns and at 50 kHz during the recording of postsynaptic currents in voltage clamp mode. Data were recorded with Clampex 10.4 (Molecular Devices) or an in-house acquisition and stimulus software (Stimulog, courtesy of Professor Zoltán Nusser, Institute of Experimental Medicine, Budapest, Hungary), and were analyzed with Clampfit 10.4 (Molecular Devices), EVAN 1.3 (courtesy of Professor Istvan Mody, Department of Neurology and Physiology, University of California, Los Angeles, CA, USA) and OriginPro 2018 (OriginLab Corp, Northampton, MA, USA).

Single-cell properties. The protocol used for recording firing patterns in current clamp mode consisted of alternating 800 ms long depolarizing and hyperpolarizing current steps with an amplitude increasing to +100 and −100 pA in 10 pA increments, then to +300 pA in 50 pA increments, and finally to 600 pA in 100 pA increments. A holding potential of −65 mV was applied during the recordings.

Paired recordings. Paired recordings with CCKBCs were performed in slices prepared from BAC-CCK-DsRed mice, whereas paired recordings with PVBCs were obtained in slices cut from BAC-PV-eGFP mice. Synaptic connections between interneurons and PNs were tested with five action potentials elicited at 33 Hz with a 5 s long interstimulus interval and were recorded for analysis with an interstimulus interval of 20 s. Series resistance (*Rs*) of the postsynaptic cell was continuously monitored and recordings in which the *Rs* exceeded 20 MΩ or changed more than 20%, or in which the analyzed features of the postsynaptic response showed changes were not included in the analysis of postsynaptic currents. Reported features of the postsynaptic currents are based on the analysis of the postsynaptic response evoked by the first action potential in each train of stimuli. The potency of synaptic connections were calculated by averaging the amplitudes of individual uPSCs excluding transmission failures, whereas the amplitude of synaptic connections was calculated by dividing the sum of the amplitudes of individual uPSCs by the number of stimulus trains (i.e. this measure includes transmission failures). Latency was measured from the peak of presynaptic action potential to the onset of the postsynaptic current, defined by 10% of the peak amplitude. Short-term plasticity was quantified on the averaged traces for each connection. Because of the possibility of low initial release probability of synapses between CCKBCs (Andrási et al., 2017), 10 action potentials were elicited at 40 Hz during paired recordings to detect synaptic connections between interneurons. To eliminate any tonic activity of CB1 receptors, which may preclude identifying homotypic CCKBC connections, these pairs were recorded in the presence of CB1 receptor antagonist AM251 (1 μM). Postsynaptic cells were clamped at −65 mV. The presence of gap junctions between interneurons was tested by injecting 800 ms long current steps into one of the recorded cells that induced hyperpolarization of at least 10 mV of amplitude, whereas simultaneous voltage deflections were monitored in the other cell in current clamp mode ($I = 0$).

Miniature excitatory postsynaptic currents (mEPSCs). Neurons recorded from BAC-CCK-DsRed or BAC-PV-eGFP mice were held at a holding potential of −65 mV in voltage clamp mode to record mEPSCs in the presence of TTX (1 μM) and gabazine (5 μM). Statistical analysis was run on data obtained from 5 CCKBCs and 5 PVBCs by comparing 110–130 mEPSCs from each cell. Events were analyzed using EVAN 1.3.

Raw data of these experiments are freely accessible (10.6084/m9.figshare.26928820).

Pharmacological experiments. The presence of inhibitory inputs on PVBCs originating from CCKBCs was tested by evoking postsynaptic currents in PVBCs by using theta electrode stimulation in brain slices prepared from BAC-PV-eGFP mice. The electrode was placed into the slice ∼200–250 μm away from the recorded PVBC, minimizing the chance of direct stimulation. The intensity of the 1 ms long stimuli was set to evoke responses with the amplitude of at least 300 pA, whereas neurons were held at −65 mV in voltage clamp mode. QX-314 was intracellularly applied to eliminate action potential generation as a result of the outward flow of Cl^- ions upon the opening of $GABA_A$ receptors. Blockade of excitatory postsynaptic currents was achieved by adding 2 mM kynurenic acid in the recording solution.

Optogenetic experiments. For testing PVBC inputs on CCKBCs, we performed whole-cell recordings simultaneously from CCKBCs and PNs in brain slices prepared from mice obtained by crossing the Pvalb-IRES-Cre with the BAC-CCK-DsRed mice. Offspring were injected with AAV5-EF1a-DIO-hChR2-eYFP (200 nL, 3.2×10^{12} vg mL^{-1}; University of North Carolina Vector Core, Chapel Hill, NC, USA; catalog no. 35 509-AAV5) in the mPFC at P120 to enable optogenetic control of local PVBC activity. ChR2 expression was allowed for 4–6 weeks before animals were killed for *in vitro* experiments. Optogenetic stimulation was achieved by three pulses of 5 ms long blue laser illumination (447 nm; Thorlabs, Newton, NJ, USA) at 20 Hz at 2.5 mW mm^{-2} intensity applied through a 40× objective. Recording postsynaptic currents at the same time from PNs and CCKBCs held at −65 mV confirmed the optical stimulation of PV+ cells to be successful in all slices.

***Post hoc* identification of cell types.** After the recordings, slices were placed into a fixative solution containing 4% paraformaldehyde in 0.1 M phosphate buffer (pH 7.4) to enable *post hoc* visualization of biocytin-filled interneurons by applying fluorophore-conjugated streptavidin (Cy3-SA or Alexa488-SA; dilution 1:10 000; Sigma-Aldrich, St Louis, MO, USA, and Molecular Probes, Eugene, OR, USA, respectively). Recorded PVBCs were distinguished from fast-spiking chandelier cells based on the morphology of their axons (Nagy-Pal et al., 2023), whereas CCKBCs showed strong DsRed expression and accommodating firing pattern. CB1 content of CCKBCs was tested with immunolabeling using rabbit anti-CB1 (Cayman, Ann Arbor, MI, USA; catalog no. 10 006 590) primary antibody at a concentration of 1:1000, revealed with Alexa405-coupled donkey anti-rabbit secondary antibody (dilution 1:500; Jackson, Bar Harbor, ME, USA). DsRed-expressing interneurons lacking CB1 immunoreactivity on their axon terminals were not included in the present study. Slices were mounted in Vectashield (Vector Laboratories) and confocal images were taken using a Nikon C2 microscope using CFI Super Plan Fluor 20× objective (NA 0.45; *z* step size: 1 μm, *xy*: 0.31 μm per pixel) and CFI Plan Apo VC 60× oil objective for higher magnification (NA 1.40; *z* step size: 0.25 μm, *xy*: 0.08 μm per pixel). BCs in different layers were divided into morphological categories defined in our recent paper (Nagy-Pal et al., 2023). PNs were identified based on their slower membrane kinetics and their distinctive firing pattern characterized by regular spiking and characteristic after-hyperpolarization.

Immunohistochemistry. For labelling putative contacts on PVBCs from CCKBCs, C57Bl6 wild type mice ($n = 3$) were deeply anaesthetized and transcardially perfused with 4% paraformaldehyde in 0.1 M phosphate buffer (pH 7.4). Then, 80 μm coronal slices containing the mPFC were prepared with a vibratome (VT1000S; Leica Microsystems). After blocking in 10% normal donkey serum, the following mixture of primary antibodies was used (3 days: first night at room temperature, then at 4°C): goat anti-CB1 (Frontier Institute Co., Ltd, Hokkaido, Japan; catalog no. CB1-Go-Af450; dilution 1:1000), mouse anti-Gephyrin (SYSY, Goettingen, Germany), #147 021; dilution 1:1000) and guinea-pig anti-PV (SYSY; catalog no. 195 004; dilution 1:5000) in 0.1 M phosphate buffer with 2% normal donkey serum and 2% Triton-X solution. Then the following mixture of secondary antibodies was used: donkey-anti-goat coupled with Alexa405, donkey-anti-mouse coupled with Alexa488 and donkey-anti-guinea-pig coupled with Alexa647 (Jackson; dilution 1:500; 4 h at room temperature). For labelling putative contacts on CCKBCs from PVBCs, mPFC slices were prepared from VGAT-IRES-Cre::BAC-CCK-GFP-coIN mice ($n = 4$) as described above. After blocking in 10% normal donkey serum, the following mixture of primary antibodies was used (2 days: first night at room temperature, then at 4°C): goat anti-CB1 (Frontier Institute; catalog no. CB1-Go-Af450; dilution 1:1000), chicken anti-GFP (SYSY; catalog no. 132 006; dilution 1:1000), mouse anti-Gephyrin (SYSY; catalog no. 147 021; dilution 1:1000) and guinea-pig anti-PV (SYSY; catalog no. 195 004; dilution 1:5000) in 0.1 M phosphate buffer with 2% normal donkey serum and 2% Triton-X solution. Then the following mixture of secondary antibodies was used: donkey-anti-goat coupled with Alexa405, donkey-anti-chicken coupled with Alexa488, donkey-anti-mouse coupled with Cy3,

donkey-anti-guinea-pig coupled with Alexa647 (Jackson; dilution 1:500; 4 h at room temperature). Slices were mounted in Vectashield (VectorLabs, Newark, CA, USA), then confocal images were taken using a Nikon microscope with CFI Plan Apo VC 60× oil objective (NA 1.40; *z* step size: 0.125 µm, *xy*: 0.08 µm per pixel). Using 3-D confocal images, interneurons within ∼30 µm depth from the surface of the slices were selected for analysis irrespective of the number of synaptic contacts on them. The surface of the somata and the putative contacts on it (i.e. where a bouton closely opposed the cell surface and a gephyrin puncta was found between them) were manually labelled and quantified with Neurolucida 10.53 (MBF Bioscience, Williston, VT, USA).

Statistical analysis

Reported features of the postsynaptic currents are based on the analysis of the first evoked response in each train of stimuli, elicited at least with an interval of 20 s. After individually measuring the features of at least 15 post-synaptic events in the case of each recorded pair, statistical tests were applied on averaged data. The potency of events was calculated by excluding, whereas amplitude was calculated by including transmission failures. To assess statistical significance in the case of datasets with non-normal distribution based on the Shapiro–Wilk test, a Mann–Whitney (M–W) *U* test was applied. Cumulative frequency distributions of mEPSC parameters were compared with a Kolmogorov–Smirnov (K–S) test. $P < 0.05$ was considered statistically significant. Statistics were performed using Origin 2018. Boxes on boxplots represent the interquartile range; filled square: mean; whiskers: 5th and 95th percentiles.

Results

In the present study, the single-cell properties and connectivity features of basket cells were investigated within the circuits of the PrL. BAC-CCK-DsRed mice were used to record CCKBCs, later identified by their CB1 immunoreactivity on their axon terminals (Fig. 1*A*), a neurochemical marker that defines this basket cell type in cortical structures together with CCK content (Bodor et al., 2005; Katona et al., 1999; Katona et al., 2001; Koukouli et al., 2022; Nagy-Pal et al., 2023; Varga et al., 2010). PVBCs sampled in BAC-PV-eGFP mice were separated from PV-expressing chandelier cells based on the morphological characteristics of their axonal arborization and bouton distribution: cartridges are formed by chandelier cell but not PVBC axonal boutons (Nagy-Pal et al., 2023). Thus, based on neuro-chemical marker expression (CCK/CB1 and PV) and morphology, we defined inhibitory interneurons in this study as CCKBCs and PVBCs.

Contrasting active and passive membrane properties of basket cells in the PrL

One of the key factors that determine the function of a given cell type is how its inputs are integrated and converted into output activity. Therefore, we first investigated the active and passive membrane properties of CCKBCs and PVBCs. Acute slices containing the PrL were prepared from BAC-CCK-DsRed or BAC-PV-eGFP mice, where CCKBCs or PVBCs express fluorescent proteins, respectively (Nagy-Pal et al., 2023), allowing their identification prior to recordings. Following *in vitro* electrophysiological recordings, *post hoc* identification based on morphology (Nagy-Pal et al., 2023) and firing pattern ensured that only BCs were included in the study (Fig. 1*A*). Analysis of voltage responses upon the injection of hyperpolarizing and depolarizing current steps revealed that CCKBCs had significantly larger input resistance (M–W, $P < 0.001$, $n_{CCKBC} = 23$ cells, $n_{PVBC} = 23$ cells from $n = 13$ and $n = 12$ animals for CCKBC and PVBC recordings, respectively), longer membrane time constant (M–W, $P < 0.001$, $n_{CCKBC} = 23$, $n_{PVBC} = 23$) and more depolarized spike threshold than PVBCs (M–W, $P < 0.001$, $n_{CCKBC} = 22$, $n_{PVBC} = 26$), but the capacitance of the two BC types was comparable (M–W, $P = 0.368$, $n_{CCKBC} = 23$, $n_{PVBC} = 23$) (Fig. 1*B* and *Ca* and Table 1). The narrow spikes of PVBCs were followed by significantly larger after-hyperpolarization potentials, and the PVBC firing pattern showed significantly less accommodation than that of CCKBCs [action potential (AP) half-width: M–W, $P < 0.001$, $n_{CCKBC} = 23$, $n_{PVBC} = 23$; AHP amplitude: M–W, $P < 0.001$, $n_{CCKBC} = 7$, $n_{PVBC} = 21$; accommodation ratio: M–W, $P < 0.001$, $n_{CCKBC} = 22$, $n_{PVBC} = 25$] (Fig. 1*B* and *C* and Table 1), a notable difference between the two BC types also found previously in other cortical areas (Barsy et al., 2017; Daw et al., 2009; Glickfeld & Scanziani 2006; Kawaguchi & Kubota 1998; Kawaguchi & Shindou 1998; Pawelzik et al., 2002; Szabo et al., 2010). Consequently, the same amount of injected current elicited firing from PVBCs with higher frequencies compared to CCKBCs and PVBCs reached higher maximum firing rate (M–W, $P < 0.001$, $n_{CCKBC} = 22$, $n_{PVBC} = 23$) (Fig. 1*Cb*), eventually unveiling their characteristic fast-spiking phenotype. These diverse membrane properties suggest that signals in the two BC types are translated into distinct activity patterns and have different integration properties in the PrL as it has been first proposed in the hippocampus (Glickfeld & Scanziani 2006).

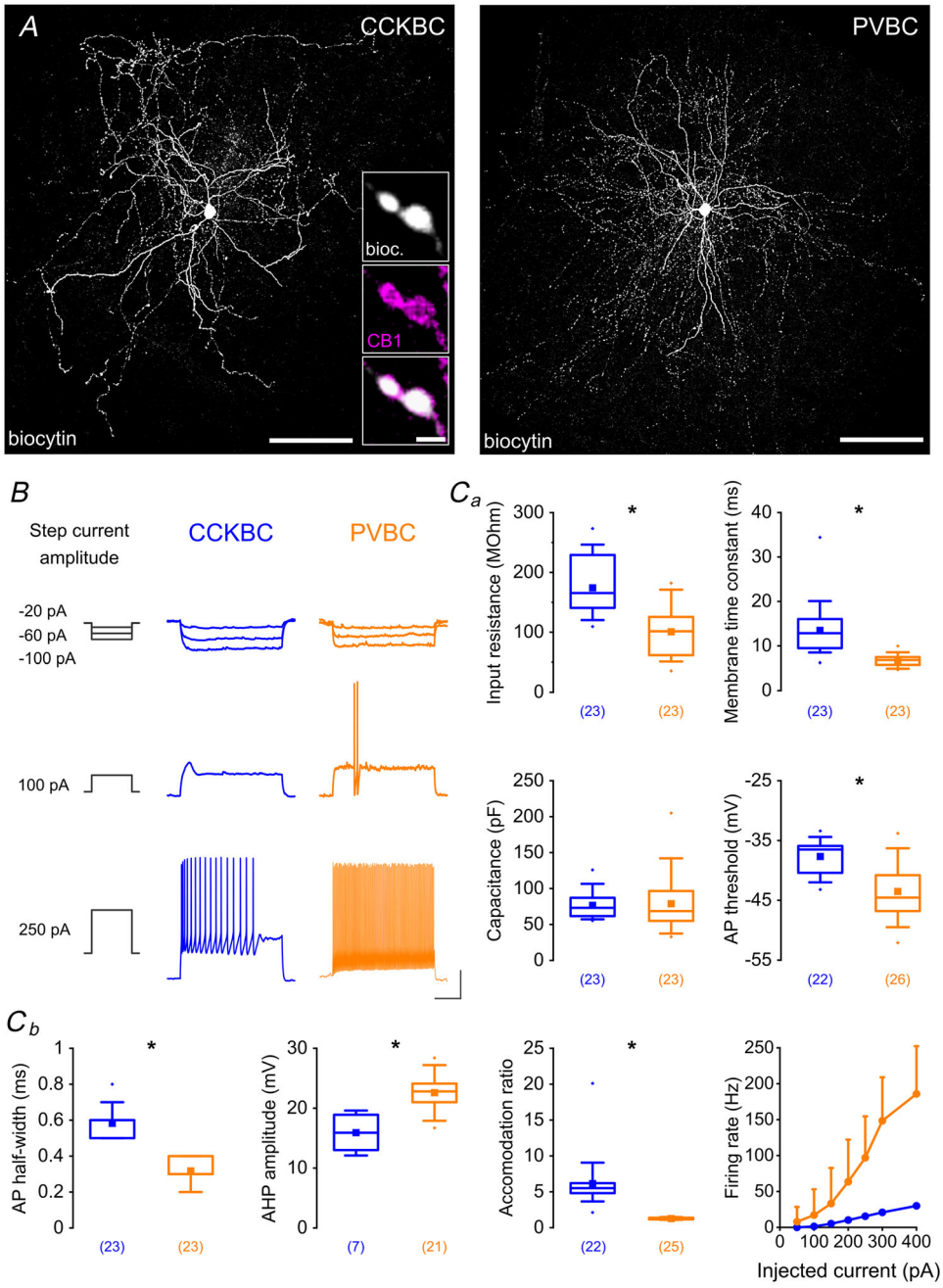

Figure 1. Analysis of *in vitro* recorded single-cell properties of basket cells reveals significant differences in their active and passive membrane features
A, confocal images taken of a biocytin-filled CCKBC and PVBC in the prelimbic cortex (PrL). Inset: Axon terminals of a CCKBC co-express CB1 and biocytin. Scale bars = 100 µm and 1 µm. *B*, representative traces of basket cell responses following current step injections. Scale bar = *x* = 200 ms, *y* = 20 mV. *Ca* and *Cb*, comparison of intrinsic electrophysiological properties uncovers substantial differences between the two basket cell types. M–W, $P = 0.368$ for capacitance, $P < 0.001$ for all the other parameters. Numbers in parentheses represent the number of analyzed recordings from $n = 13$ BAC-CCK-DsRed and $n = 12$ BAC-PV-eGFP mice for CCKBC and PVBC recordings, respectively. Details are provided in Table 1. Boxes in this and other figures represent the interquartile range; filled square: mean; whiskers: 5th and 95th percentiles.

Table 1. Summary of single-cell features, properties of uPSCs and mEPSCs

		CCKBC		PVBC			
	Parameters	median (first and third quartile)	*n*	median (first and third quartile)	*n*	*P* value	Statistical test
Single-cell properties	Input resistance (MΩ)	165.5 (140.6, 229.1)	23	101.5 (61.55, 125.5)	23	< **0.001**	MW
	MTC (ms)	12.85 (9.49, 16.04)	23	6.83 (5.78, 7.47)	23	< **0.001**	MW
	Capacitance (pF)	73.11 (61.63, 87.13)	23	68.58 (54.97, 96.53)	23	0.368	MW
	AP threshold (mV)	−36.5 (−40.4, −35.9)	22	−44.55 (−46.8, −40.8)	26	< **0.001**	MW
	AP half-width (ms)	0.6 (0.5, 0.6)	23	0.3 (0.3, 0.4)	23	< **0.001**	MW
	AHP amplitude	15.9 (13, 18.9)	7	22.8 (21, 24.1)	21	< **0.001**	MW
	Accomodation ratio	5.51 (4.81, 6.2)	22	1.27 (1.15, 1.38)	25	< **0.001**	MW
	Max. firing rate (Hz)	41.9 (31.3, 48.8)	22	208.8 (171.3, 228.8)	23	< **0.001**	MW
uEPSC	Potency (pA)	17.27 (16.06, 19.8)	13	60.56 (35.04, 84.46)	20	< **0.001**	MW
	Amplitude (pA)	15.09 (13.02, 17.4)	13	50.89 (27.95, 84.46)	20	< **0.001**	MW
	Failure rate	0.12 (0.03, 0.19)	13	0.06 (0, 0.16)	20	0.523	MW
	Latency (ms)	1.23 (0.84, 1.8)	12	0.64 (0.48, 0.82)	18	< **0.001**	MW
	RT 10–90% (ms)	0.79 (0.38, 0.81)	13	0.3 (0.21, 0.35)	20	< **0.001**	MW
	T50 (ms)	2.86 (1.68, 3.5)	12	1.29 (0.84, 1.71)	18	< **0.001**	MW
mEPSC	Instantaneous rate (s^{-1})	10.91 (5.42, 25.46)	622	20.42 (9.18, 48.79)	626	< **0.001**	KS
	Amplitude (pA)	15.83 (13.2, 20.52)	617	28.48 (18.68, 44.89)	616	< **0.001**	KS
	RT 20–80% (ms)	0.44 (0.25, 0.66)	613	0.21 (0.13, 0.34)	612	< **0.001**	KS
	Decay time constant (ms)	1.99 (1.96, 2.5)	5	1.33 (1.29, 1.41)	5	**0.0216**	MW
uIPSC	Potency (pA)	29.83 (16.65, 60.18)	19	38.21 (29.96, 120.62)	21	0.0617	MW
	Amplitude (pA)	18.71 (9.39, 38.3)	19	38.21 (29.8, 120.62)	21	**0.00446**	MW
	Failure rate	0.35 (0.08, 0.5)	19	0 (0, 0.06)	21	< **0.001**	MW
	Latency (ms)	1.38 (0.98, 1.71)	19	0.71 (0.63, 0.83)	21	< **0.001**	MW
	RT 10–90% (ms)	0.61 (0.53, 0.75)	17	0.58 (0.47, 0.66)	21	0.0859	MW
	T50 (ms)	4.55 (3.34, 5.55)	16	4.08 (3.31, 4.95)	21	0.5602	MW
Homotypic connections	Potency (pA)	26.7 (21.07, 37.53)	4	33.28 (28, 116.85)	6	0.241	MW
	Failure rate	0.62 (0.5, 0.65)	5	0.03 (0, 0.09)	6	**0.0129**	MW
	Latency (ms)	1.02 (0.9, 1.36)	4	0.64 (0.44, 1.06)	6	0.166	MW

Data are presented as the median with the first and third quartiles in parentheses. *P* values below the level of significance are in bold. AP, action potential; AHP, afterhyperpolarization; KS, Kolmogorov-Smirnov test; mEPSC, miniature excitatory postsynaptic current; MTC, membrane time constant; MW, Mann-Whitney test; RT, rise time, uEPSC, unitary excitatory postsynaptic current; uIPSC, unitary inhibitory postsynaptic current.

Local PNs evoke larger uEPSCs in PVBCs with short latency and fast kinetic properties

To determine how the two BC types are embedded into the local excitatory networks, we investigated the excitatory connections between PNs and BCs by performing paired recordings and analyzed the properties of the unitary excitatory postsynaptic currents (uEPSCs) evoked by the first action potential in each spike train (Fig. 2*A* and *B* and Table 1). Our recordings revealed that uEPSCs evoked in PVBCs have significantly larger amplitude than those evoked in CCKBCs (potency: M–W, $P < 0.001$, $n_{\mathrm{CCKBC}=}13$ pairs, $n_{\mathrm{PVBC}=}20$ pairs from $n = 17$ and $n = 15$ animals for CCKBC and PVBC recordings, respectively; amplitude: M–W, $P < 0.001$, $n_{\mathrm{CCKBC}=}13$, $n_{\mathrm{PVBC}=}20$) (Fig. 2*C* and Table 1). Moreover, uEPSCs in PVBCs followed the presynaptic action potentials with significantly shorter latency than those in CCKBCs (M–W, $P < 0.001$, $n_{\mathrm{CCKBC}=}12$, $n_{\mathrm{PVBC}=}18$) (Fig. 2*C* and Table 1), suggesting that, over the course of the first milliseconds after the activation of PNs, local excitatory signals reach different BC populations. Besides this temporal preference for exciting PVBCs, release from excitatory synapses to CCKBCs or PVBCs were found to be similarly successful (failure rate: M–W, $P = 0.523$, $n_{\mathrm{CCKBC}=}13$, $n_{\mathrm{PVBC}=}20$). Kinetic properties of uEPSCs recorded from CCKBCs, however, were significantly slower both in terms of their 10–90% rise time and half-width of events, the time span measured at the half-amplitude (T50) (rise time 10–90%: M–W, $P < 0.001$, $n_{\mathrm{CCKBC}=}13$, $n_{\mathrm{PVBC}=}20$; T50:

M–W, $P < 0.001$, $n_{CCKBC} = 12$, $n_{PVBC} = 18$), especially in the case of CCKBCs in L2/3 (Fig. 2*C* and Tables 1–3). We also observed uEPSCs with slightly slower kinetics on L2/3 PVBCs compared to PVBCs in deeper layers, but these were the only interlaminar differences we observed within the two BC types (Tables 2 and 3).

Synaptic connections are characterized by diverse dynamics at the short-term time scale that are dependent on the pre- and postsynaptic partners (Ali et al., 1998; Reyes et al., 1998). To unravel whether excitatory synapses on BCs become potentiated or depressed during sustained presynaptic activation we delivered trains of square pulses to evoke five action potentials at 33 Hz and compared the amplitude of the postsynaptic currents recorded in BCs (Fig. 2*D*). The amplitude of uEPSCs in PVBCs received from local PNs did not decrease considerably and remained in the 80–106% range of the first uEPSC on average (second uEPSC: 106.65 ± 5.19% and fifth uEPSC: 78.2 ± 6.03%). Conversely, CCKBCs were found to be innervated by depressing excitatory synapses, as the amplitude of the second and fifth uEPSCs decreased on average to 58.97 ± 5.52% and 29.53 ± 3.03% of the first uEPSC, respectively. The probability of finding a connection between PNs and BCs also differed between BC types ($P = 0.0343$, Fisher's exact test) (Fig. 2*E*) in agreement with previous studies (Andrasi et al., 2017; Lu et al., 2017). Taken together, our data suggest that the excitation generated within the prelimbic networks distinguishes between the two types of BCs in a number of aspects: PVBCs receive larger and faster synaptic excitation that is maintained if repetitive firing in PNs is induced, whereas the local PN population gives rise to smaller and slower postsynaptic events in CCKBCs that show prominent depression when trains of action potentials are evoked in PNs.

Kinetic properties of mEPSCs

To address whether the different kinetic properties of uEPSCs from neighboring PNs were a general feature

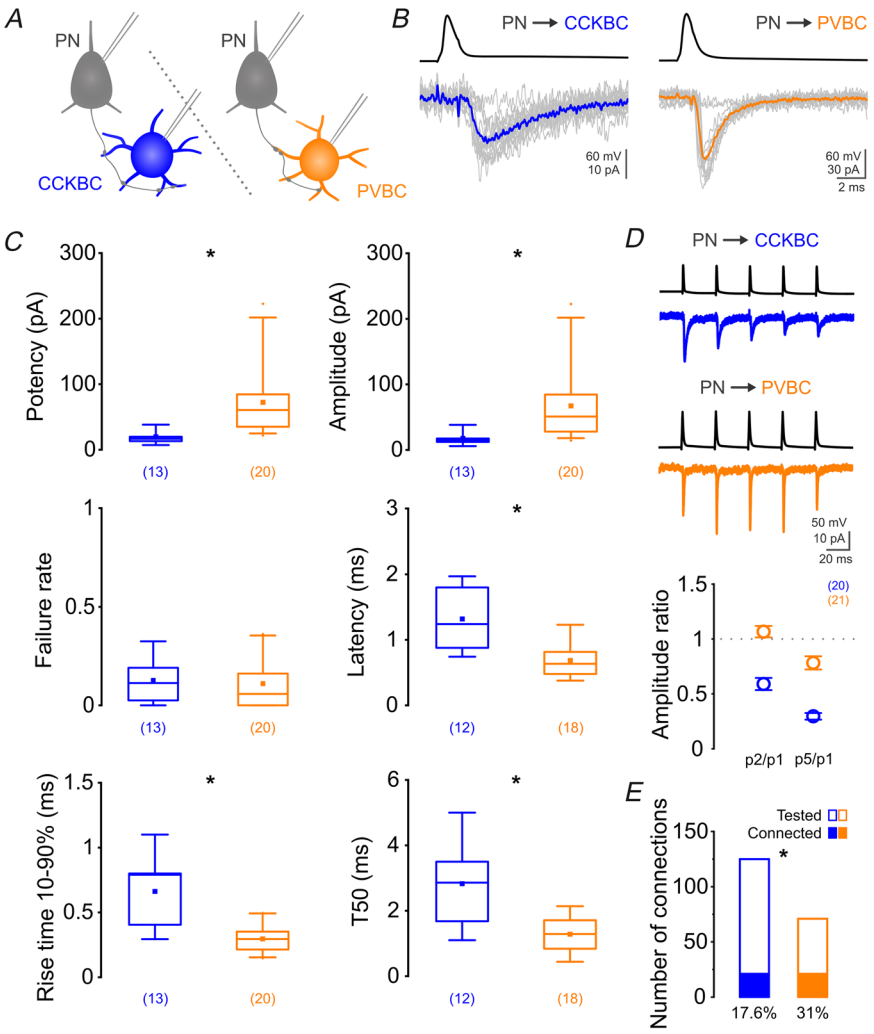

Figure 2. Paired recordings between PNs and BCs unveil larger uEPSCs in PVBCs exhibiting faster kinetics than uEPSCs in CCKBCs
A, schematic illustration of the experiment. *B*, representative traces of the first evoked AP in a train of five APs in PNs (top) and the postsynaptic uEPSCs recorded in BCs (bottom). Fifteen consecutive traces in grey, average in colour. *C*, comparison of the main properties of the first uEPSCs. M–W, $P = 0.523$ for failure rate, $P < 0.001$ for all the other parameters. Numbers in parentheses represent the number of analyzed recordings from $n = 17$ BAC-CCK-DsRed and $n = 15$ BAC-PV-eGFP mice for CCKBC and PVBC recordings, respectively. Details are provided in Table 1. *D*, representative traces of synapse type-dependent short-term plasticity revealed by five evoked APs in the presynaptic cell (top, middle). Ratio of the amplitude of the second and first (2/1) or the fifth and first (5/1) uEPSCs summarizes the short-term dynamics of the excitatory connections between PNs and BCs (bottom). Data are presented as the mean ± SEM. Numbers in parentheses represent the number of analyzed recordings from $n = 17$ BAC-CCK-DsRed and $n = 15$ BAC-PV-eGFP mice for CCKBC and PVBC recordings, respectively. *E*, connection probability is significantly larger between PNs and PVBCs than between PNs and CCKBCs ($P = 0.0346$, Fisher's exact test).

Table 2. Features of uEPSC and uIPSC based on the layer where BCs were located

		uEPSC by layers		uIPSC by layers	
Parameter	Cell type	n	median (1st and 3rd quartile)	n	median (1st and 3rd quartile)
Potency (pA)	$CCKBC_{sup}$	6	14.74 (11.65, 18.13)	9	16.65 (10.66, 41.26)
	$CCKBC_{deep}$	7	17.41 (16.2, 36.7)	10	40.73 (29.45, 60.18)
	$PVBC_{L2/3}$	7	58.73 (28.22, 88.94)	7	50.84 (33.06, 210.11)
	$PVBC_{L5a}$	5	64.65 (50.4, 79.98)	9	32.5 (24.71, 58.93)
	$PVBC_{L5b}$	8	54.16 (35.04, 83.64)	5	85.19 (29.8, 120.62)
Amplitude (pA)	$CCKBC_{sup}$	6	14.28 (9.43, 17.4)	9	15.81 (7.94, 27.5)
	$CCKBC_{deep}$	7	15.09 (14.4, 25.69)	10	27.33 (15.84, 38.3)
	$PVBC_{L2/3}$	7	57.59 (27.61, 88.94)	7	50.84 (31.25, 210.11)
	$PVBC_{L5a}$	5	64.65 (50.4, 79.98)	9	30.95 (16.94, 58.93)
	$PVBC_{L5b}$	8	43.27 (26.65, 73.15)	5	85.19 (29.8, 120.62)
Failure rate	$CCKBC_{sup}$	6	0.06 (0, 0.19)	9	0.33 (0.05, 0.48)
	$CCKBC_{deep}$	7	0.13 (0.11, 0.26)	10	0.36 (0.2, 0.5)
	$PVBC_{L2/3}$	7	0.02 (0, 0.13)	7	0 (0, 0.06)
	$PVBC_{L5a}$	5	0 (0, 0.05)	9	0 (0, 0.12)
	$PVBC_{L5b}$	8	0.14 (0.05, 0.33)	5	0 (0, 0)
Latency (ms)	$CCKBC_{sup}$	6	1.52 (1.22, 1.82)	9	1.36 (1.06, 2.11)
	$CCKBC_{deep}$	6	0.96 (0.76, 1.26)	10	1.43 (0.97, 1.52)
	$PVBC_{L2/3}$	7	0.64 (0.48, 1.1)	7	0.71 (0.52, 0.8)
	$PVBC_{L5a}$	3	0.7 (0.63, 0.82)	9	0.66 (0.62, 0.74)
	$PVBC_{L5b}$	8	0.51 (0.47, 0.77)	5	0.83 (0.77, 0.88)
Rise time 10-90% (ms)	$CCKBC_{sup}$	6	0.81 (0.8, 1.1)	8	0.67 (0.54, 0.82)
	$CCKBC_{deep}$	7	0.41 (0.34, 0.79)	9	0.59 (0.52, 0.73)
	$PVBC_{L2/3}$	7	0.41 (0.29, 0.49)	7	0.5 (0.39, 0.57)
	$PVBC_{L5a}$	5	0.33 (0.28, 0.34)	9	0.59 (0.56, 0.61)
	$PVBC_{L5b}$	8	0.21 (0.18, 0.27)	5	0.66 (0.63, 0.66)
T50 (ms)	$CCKBC_{sup}$	6	3.5 (3.2, 4.9)	7	5.3 (3.4, 5.88)
	$CCKBC_{deep}$	6	1.68 (1.67, 2)	9	4.2 (3.28, 5.07)
	$PVBC_{L2/3}$	7	1.73 (1.58, 1.94)	7	4.08 (2.85, 4.95)
	$PVBC_{L5a}$	4	1.26 (1.07, 1.44)	9	3.9 (3.12, 4.55)
	$PVBC_{L5b}$	7	0.75 (0.58, 1.28)	5	4.43 (4.11, 5.6)
p2/p1	$CCKBC_{sup}$	10	0.4 (0.33, 0.78)	11	0.84 (0.69, 1.22)
	$CCKBC_{deep}$	10	0.64 (0.38, 0.85)	13	0.94 (0.65, 1.17)
	$PVBC_{L2/3}$	8	1.09 (0.95, 1.23)	10	0.64 (0.6, 0.7)
	$PVBC_{L5a}$	5	0.97 (0.87, 1.38)	8	0.71 (0.6, 0.92)
	$PVBC_{L5b}$	8	1.04 (0.8, 1.28)	5	0.77 (0.68, 0.82)
p5/p1	$CCKBC_{sup}$	10	0.21 (0.15, 0.37)	11	0.89 (0.8, 1.55)
	$CCKBC_{deep}$	10	0.31 (0.22, 0.41)	13	0.96 (0.52, 1.13)
	$PVBC_{L2/3}$	8	0.88 (0.73, 1.11)	10	0.39 (0.35, 0.46)
	$PVBC_{L5a}$	5	0.65 (0.44, 0.96)	8	0.5 (0.36, 0.6)
	$PVBC_{L5b}$	8	0.61 (0.49, 0.85)	5	0.55 (0.42, 0.64)

CCKBCsup, superficial CCKBCs with their somata in L2/3; CCKBCdeep, CCKBCs with their somata in layer 5a or 5b. PVBCL2/3, PVBCL5a, PVBCL5b, PVBCs with their somata in the corresponding layer (Nagy-Pal et al., 2023).

of excitation arriving onto BCs in the PrL, we recorded mEPSCs in the two BC types in the presence of TTX (1 μM) and gabazine (5 μM) to block voltage-gated Na^+ channels and $GABA_A$ receptors, respectively (Fig. 3*A* and *B*). Comparison of a similar number of recorded events (110–130 mEPSCs) from each cell revealed that PVBCs received mEPSCs at a higher rate (K–S, $P < 0.001$, $n_{CCKBC} = 622$ events from five cells, $n_{PVBC} = 626$ events from five cells from $n = 2$ and $n = 2$ animals for CCKBC and PVBC recordings, respectively) and these events had larger peak amplitudes than those arriving on CCKBCs (K–S, $P < 0.001$, $n_{CCKBC} = 617$, $n_{PVBC} = 616$) (Fig. 3*C* and Table 1). The rise time 20–80% of miniature events on CCKBCs were slower, similarly to the unitary events evoked in paired recordings (K–S, $P < 0.001$, $n_{CCKBC} = 613$, $n_{PVBC} = 612$) (Fig. 3*C* and Table 1).

Table 3. Results of statistical tests comparing uPSC features based on the layer where BCs were located

		CCKBC			PVBC						
		n		*P* value (M–W test)	*n*			*P* value (K–W analysis of variance)	Dunn's test		
PSC	Parameter	Superficial	Deep		L2/3	L5a	L5b		L2/3 *vs.* L5a	L2/3 *vs.* L5b	L5a *vs.* L5b
uEPSC	Potency (pA)	6	7	0.225	7	5	8	0.976	–	–	–
	Amplitude (pA)	6	7	0.52	7	5	8	0.774	–	–	–
	Failure rate	6	7	0.429	7	5	8	0.162	–	–	–
	Latency (ms)	6	6	0.174	7	3	8	0.608	–	–	–
	RT 10–90% (ms)	6	7	**0.008**	7	5	8	**0.023**	1	**0.026**	0.188
	T50 (ms)	6	6	**0.008**	7	4	7	**0.002**	0.275	**0.001**	0.578
	p2/p1	10	10	0.162	8	5	8	0.853	–	–	–
	p5/p1	10	10	0.307	8	5	8	0.092	–	–	–
uIPSC	Potency (pA)	9	10	0.131	7	9	5	0.43	–	–	–
	Amplitude (pA)	9	10	0.348	7	9	5	0.375	–	–	–
	Failure rate	9	10	0.54	7	9	5	0.205	–	–	–
	Latency (ms)	9	10	0.653	7	9	5	0.16	–	–	–
	RT 10–90% (ms)	8	9	0.47	7	9	5	0.093	–	–	–
	T50 (ms)	7	9	0.244	7	9	5	0.463	–	–	–
	p2/p1	11	13	0.954	10	8	5	0.144	–	–	–
	p5/p1	11	13	0.247	10	8	5	**0.043**	0.2	0.066	1

For data, see Table 2. *P* values below the level of significance are in bold.

Furthermore, peak scaled averages also demonstrate the slower decay of mEPSCs recorded in CCKBCs (Fig. 3*D*), confirmed by the decay time constant assessed on the averaged events in case of each recorded cell (M–W, $P = 0.0216$, $n_{CCKBC} = 5$, $n_{PVBC} = 5$) (Fig. 3*E* and Table 1). These results suggest that the differential kinetic properties of excitatory postsynaptic events obtained in paired recordings are not a result of sampling biases in our data but reflect the distinct features of local excitatory inputs on the two BC types.

PVBCs innervate local PNs with reliable but depressing synapses

The influence of BCs on prelimbic processes is largely determined by their impact on postsynaptic partners. To uncover the effect of single BCs on neighboring PNs in the PrL we performed paired recordings between BCs and PNs (Fig. 4*A* and *B*). Action potentials evoked in PVBCs elicited unitary inhibitory postsynaptic currents (uIPSCs) in PNs with significantly larger amplitude than those evoked by CCKBC spikes, although the potency did not differ significantly (potency: M–W, $P = 0.0617$; amplitude: M–W, $P = 0.00446$, $n_{CCKBC} = 19$ pairs, $n_{PVBC} = 21$ pairs from $n = 17$ and $n = 16$ animals for CCKBC and PVBC recordings, respectively) (Fig. 4*C* and Table 1). Although PVBC synapses were highly reliable, almost every third action potential in CCKBCs failed to evoke a uIPSC in PNs, leading to a significant difference between the failure rates of the two synapse types (M–W, $P < 0.001$, $n_{CCKBC} = 19$, $n_{PVBC} = 21$). Notably, postsynaptic events upon PVBC discharges showed significantly shorter latency than those following CCKBC activation (M–W, $P < 0.001$, $n_{CCKBC} = 19$; $n_{PVBC} = 21$) (Fig. 4*C* and Table 1), similarly to that found previously (Galarreta et al., 2008). Nonetheless, the two BC types evoke postsynaptic events in PNs with similar kinetics both in terms of their 10–90% rise time (M–W, $P = 0.0859$, $n_{CCKBC} = 17$, $n_{PVBC} = 21$) and T50 (M–W, $P = 0.5602$, $n_{CCKBC} = 16$, $n_{PVBC} = 21$) (Table 1). Furthermore, we found no significant differences in the features of uIPSCs evoked by BCs located in different layers (Tables 2 and 3).

Investigation of the short-term dynamics in these inhibitory synapses with the same protocol described above revealed that synapses arriving from PVBCs onto PNs showed significant short-term depression (second and fifth uIPSC amplitude decreased to 71.4 ± 3.4% and 46.27 ± 2.62% of the first response), a phenomenon previously observed in other cortical regions as well (Barsy et al., 2017; Galarreta & Hestrin 1998; Hefft & Jonas 2005; Szabo et al., 2010) (Fig. 4*D*). On the other hand, uIPSCs evoked by CCKBCs became neither potentiated, nor depressed (90.68 ± 5.6% and 100.85 ± 8.29% of the first response) (Galarreta et al., 2008; Hefft & Jonas 2005) (Fig. 4*D*). Additionally, PNs were innervated by nearby PVBCs with significantly higher probability than by CCKBCs ($P = 0.0248$, Fisher's exact test) (Fig. 4*E*). Taken together, our results indicate that PVBC spikes reliably evoke larger postsynaptic currents than CCKBCs in PNs, but in case of prolonged BC activation, PNs can receive a steadier level of inhibition from CCKBCs.

Basket cells form chemical synapses and gap junctions with their own cell type

Electrical synapses between neurons of the same inhibitory cell type are generally common in cortical circuits (Andrasi et al., 2017; Galarreta & Hestrin 1999; Gibson et al., 1999; Tamas et al., 2000), whereas the preference of inhibitory neurons for establishing homotypic chemical synapses is cell type-dependent (Pfeffer et al., 2013; Tremblay et al., 2016). To reveal the extent to which BCs are synaptically interconnected and the electrophysiological properties of their contacts in the PrL, we performed paired recordings between the same type of BCs (Fig. 5*A*). Testing electrical coupling was conducted by injecting hyperpolarizing current steps in one of the cells when recording membrane potential changes in the other cell (Fig. 5*B*, top). Chemical synapses were tested by eliciting 10 action potentials (Fig. 5*B*, bottom). CCKBCs were frequently coupled electrically (16/23 tests, 69.6%, from $n = 7$ animals) but chemical connections seemed less numerous between them (9/31 tests, 29%), despite the elimination of any tonic activation of CB1 by AM251 application (1 μM). By contrast, every second recorded PVBC evoked uIPSCs in other PVBCs in paired recordings (13/25 tests, 52%, from $n = 7$ animals) but only 25% of the tested cells were connected via gap junctions (2/8 tests) (Fisher's exact test, $P = 0.0429$ and $P = 0.103$ for gap junctions and chemical synapses, respectively).

In terms of the main properties of the chemical connections, uIPSCs evoked by the first action potential tended to have larger potency in synapses between PVBCs (M–W, $P = 0.241$, $n_{CCKBC} = 4$ pairs, $n_{PVBC} = 6$ pairs) (Fig. 5*D* and Table 1). Although there was a tendency for uIPSCs evoked by CCKBC spikes to start off with larger latency than uIPSCs in homotypic PVBC synapses, the difference did not reach significance (M–W, $P = 0.166$, $n_{CCKBC} = 4$, $n_{PVBC} = 6$) (Fig. 5*D* and Table 1). On the other hand, the rate of failure for the first action potential was significantly higher for CCKBC than for PVBC synapses (M–W, $P = 0.0129$, $n_{CCKBC} = 5$, $n_{PVBC} = 6$) (Fig. 5*D* and Table 1), suggesting a more reliable neurotransmission between the latter BCs. A sustained presynaptic activity, however, revealed that homotypic CCKBC synapses display strong facilitation, whereas PVBCs receive uIPSCs of decreasing amplitude (Fig. 5*E*). Taken together, homotypic BC pairs display different synaptic characteristics and connectivity patterns in the PrL.

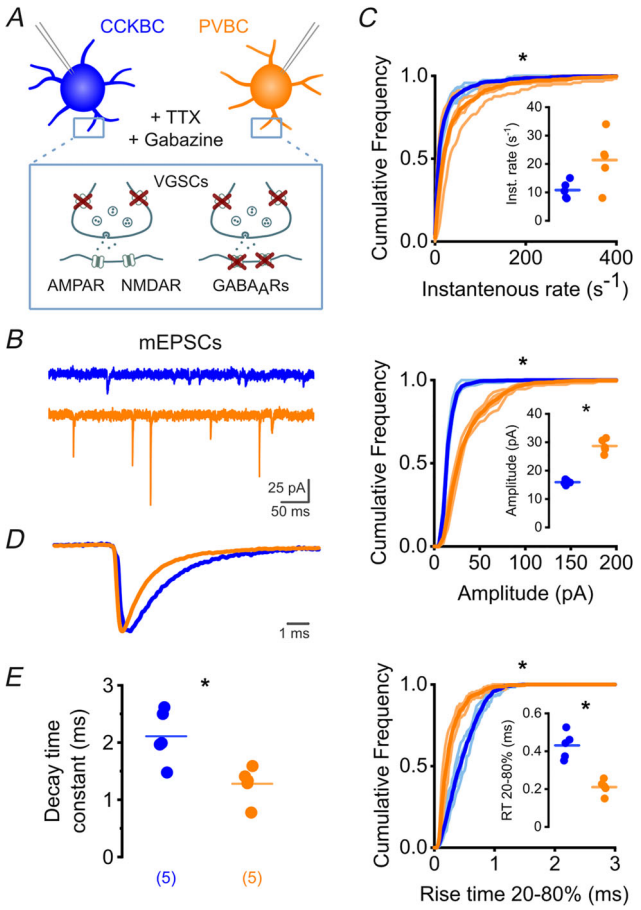

Figure 3. Differences in the kinetics of mEPSCs recorded in BCs resemble the uEPSCs evoked in paired recordings
A, mEPSCs recorded in BCs in the presence of TTX (1 μM) and gabazine (5 μM) to block voltage-gated sodium channels (VGSCs) and $GABA_A$ receptors ($GABA_A$Rs). *B*, representative traces of recordings obtained in the two BC types. *C*, cumulative frequency plots showing that PVBCs receive miniature events with higher instantaneous rate (top), amplitude (middle) and exhibit faster rise time kinetics (bottom). Thin lines represent data from individual cells; thick lines represent pooled data from $n = 2$ BAC-CCK-DsRed mice for CCKBC and $n = 2$ BAC-PV-eGFP mice for PVBC recordings, $n = 5$ cells for both cell types. K–S test on pooled datasets, $P < 0.001$ for all parameters. Insets: median values of mEPSC parameters obtained in each cell ($n = 5$ for both cell types). Inst. rate: M–W, $P = 0.0947$, amplitude: M–W, $P = 0.0122$; rise time 20–80%: M–W, $P = 0.0122$. Details are provided in Table 1. *D*, normalized averages of mEPSCs recorded in CCKBCs and PVBCs ($n = 5$ for both cell types) demonstrate the slower decay kinetics of mEPSCs recorded in CCKBCs. *E*, mEPSCs in CCKBCs on average are characterized by longer decay time constants. Data points represent decay time constants measured on the averages of mEPSCs recorded in individual cells ($n = 5$ cells for both cell types, M–W, $P = 0.0216$).

The two basket cell types are interconnected

Previous studies have shown that the two BC types are interconnected in the hippocampus (Dudok et al., 2021) but not in the amygdala (Andrasi et al., 2017). To determine the presence or absence of functional synaptic connections on PVBCs established by CCKBCs in the PrL, we used a pharmacological approach and took advantage of CB1 expression on CCKBC axon terminals (Nagy-Pal et al., 2023) (Fig. 1*A*) that is selective for this cell type among cortical inhibitory neurons (Bodor et al., 2005). Extracellular stimulation was used to evoke IPSCs in

PVBCs (Fig. 6*A*), whereas glutamatergic synaptic transmission was blocked by 2 mM kynurenic acid applied in the external solution. Bath application of the CB1 agonist WIN55,212-2 (1 μM) reduced the amplitude of evoked postsynaptic currents in the recorded cells below 50% of the initial amplitude values ($n = 3$ cells from $n = 3$ animals) (Fig. 6*B*), demonstrating the presence of CB1-sensitve inputs to PVBCs. These electrophysiological data were further supported by our anatomical results showing CB1+ axonal boutons opposed to the majority of sampled PV+ somata (29 out of $n = 33$ cells, 87.9%, from $n = 3$ animals) (Fig. 6*C* and *D*). Immunostaining against gephyrin (the anchoring protein of $GABA_A$ receptors) (Sassoe-Pognetto & Fritschy 2000) was used to ensure that only inhibitory synapses are included in the quantification. Taken together, our two independent approaches provide evidence that CB1-sensitive inputs from CCKBCs are present on PVBCs.

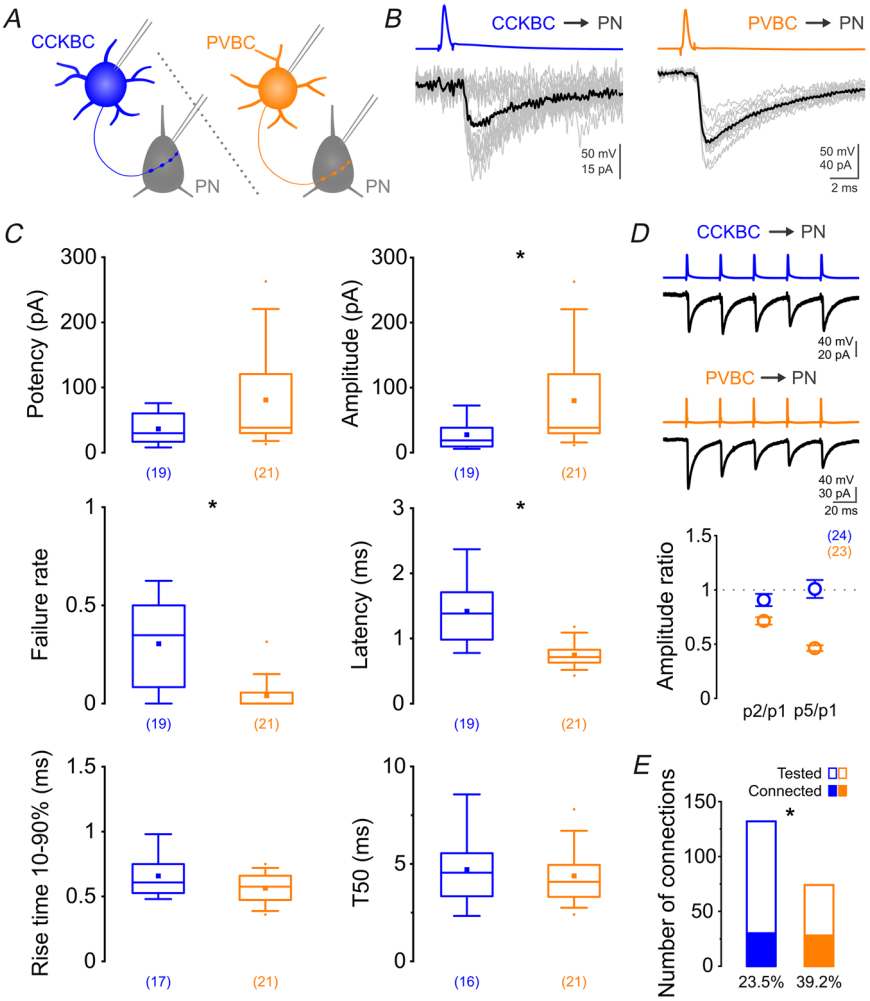

Figure 4. Paired recordings between BCs and PNs reveal the strong but depressing nature of synaptic inhibition arriving from PVBCs compared to uIPSCs evoked by CCKBCs
A, schematic illustration of the experiment. *B*, representative traces of the first presynaptic AP in a train of five APs evoked in BCs (top) and the postsynaptic uIPSCs recorded in PNs (bottom). Fifteen consecutive traces in grey, average in black. *C*, comparison of the main properties of the first uIPSCs. Numbers in parentheses represent the number of analyzed recordings from $n = 17$ BAC-CCK-DsRed and $n = 16$ BAC-PV-eGFP mice for CCKBC and PVBC recordings, respectively. *P* values for M–W tests: potency: $P = 0.0617$; amplitude: $P = 0.00446$; failure rate: $P < 0.001$; latency: $P < 0.001$; rise time 10–90%: $P = 0.0859$; T50: $P = 0.5602$. Details are provided in Table 1. *D*, representative traces of synapse type-dependent short-term plasticity revealed by eliciting five APs in the presynaptic cell (top, middle). Ratio of the amplitude of the second and first (2/1) or the fifth and first (5/1) uIPSC summarizes the short-term dynamics of the inhibitory connections between BCs and PNs (bottom). Data are presented as the mean ± SEM. Numbers in parentheses represent the number of analyzed recordings from $n = 17$ BAC-CCK-DsRed and $n = 16$ BAC-PV-eGFP mice for CCKBC and PVBC recordings, respectively. *E*, PNs were found to be innervated by PVBCs significantly more frequently than by CCKBCs ($P = 0.0248$, Fisher's exact test).

To investigate the potential synaptic connections established by PVBCs on CCKBCs, we crossed BAC-CCK-DsRed mice with PV-Cre mice. Therefore, in offspring, we could target fluorescence labelled CCKBCs (Nagy-Pal et al., 2023) and activate PVBCs using optogenetics in the same preparations. After 4–6 weeks following the injection of AAV5-EF1-DIO-hChR2-eYFP into the PrL, we prepared acute slices and recorded from CCKBCs and PNs simultaneously in whole-cell configuration (Fig. 7*A*). The cell types of the recorded neurons were verified by *post hoc* immunostaining against biocytin and CB1. Successful optogenetic activation of the PV+ population upon light stimulation was evident from the large IPSCs evoked in PNs (Fig. 7*B*), whereas recorded CCKBCs also received prominent inhibition without exception. The amplitude of these inhibitory currents varied between cells and cell types as well (M–W, $P < 0.001$, $n_{CCKBC} = 14$ cells, $n_{PN} = 10$ cells from $n = 3$ animals) but the mean amplitude of IPSCs recorded from CCKBCs reached 11.1% of the IPSCs evoked simultaneously in PNs on average (Fig. 7*B*). Latency of the responses measured from the beginning of light illumination was significantly larger for CCKBCs than for PNs (M–W, $P = 0.02062$, $n_{CCKBC} = 14$, $n_{PN} = 10$) (Fig. 7*B*). In addition to these experiments, we also identified PV+ inhibitory synaptic contacts on the somata of CCKBCs in slices containing the PrL prepared from the offspring generated by crossing VGAT-IRES-Cre and BAC-CCK-GFP-coIN mice (Fig. 7*C*). Immunostaining against PV and gephyrin revealed that the majority of the CCK/GFP+ somata received PV+ input (27 out of $n = 32$ cells, 84.4% from $n = 4$ animals) (Fig. 7*D*). In summary, these results demonstrate the innervation between the two BC types in the PrL.

Discussion

Based on our electrophysiological and anatomical data summarized in Fig. 8, we determined the properties of synaptic transmission between PNs and BCs in the mouse PrL and provided evidence regarding the connectivity among the two BC types. We showed that the membrane properties of BCs and synaptic connections with PNs display cell type specific characteristics. Our paired recordings revealed that PNs located in the PrL not only evoke larger unitary excitatory currents in PVBCs than in CCKBCs, but also these currents have shorter latency and faster kinetic parameters. Inhibition provided by PVBCs to PNs followed presynaptic activation more

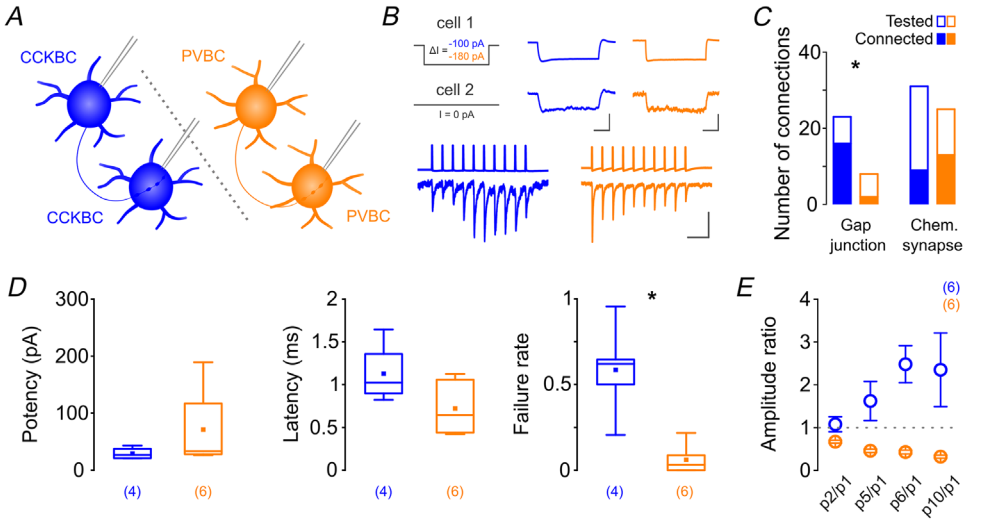

Figure 5. Paired recordings from homotypic BCs demonstrate that BCs innervate their own kind with chemical synapses and gap junctions as well
A, schematic illustration of the experiment. *B*, example traces of gap junctions revealed by injecting hyperpolarizing current steps into one of the recorded cells, averages of 50 consecutive traces (top). Example traces of recorded chemical synapses between the same type of BCs, averages of 10 consecutive traces (bottom). Scale bars: gap junctions: CCKBC *x*: 20 mV, 1 mV; *y*: 200 ms; PVBC: *x*: 15 mV, 0.5 mV; *y*: 200 ms; chemical synapses: *x*: CCKBC: 70 mV, 20 pA; PVBC: 70 mV, 50 pA; *y*: 50 ms. *C*, comparison of connection probabilities. Filled bars represent the number of connections, empty bars represent the number of tests ($P = 0.0429$ and $P = 0.103$ for gap junctions and chemical synapses, respectively, Fisher's exact test). *D*, features of the first postsynaptic responses in homotypic connections between CCKBCs and PVBCs. Numbers in parentheses represent the number of analyzed recordings from $n = 7$ BAC-CCK-DsRed and $n = 7$ BAC-PV-eGFP mice for CCKBC and PVBC recordings. *P* values for M–W tests: potency: $P = 0.241$; latency: $P = 0.166$; failure rate: $P = 0.0129$. *E*, ratio of the amplitude of the second, fifth, sixth and tenth uIPSC to the first response summarizes the short-term dynamics of the inhibitory connections between homotypic BCs. Data are presented as the mean ± SEM.

rapidly and reliably than the uIPSCs evoked by CCKBC firing, which also tended to result in unitary currents of smaller amplitude. We provided anatomical and electrophysiological evidence that BCs innervate not only their own kind, but also establish functional connections with the other BC type, a circuit motif highly relevant to our understanding of cell type function.

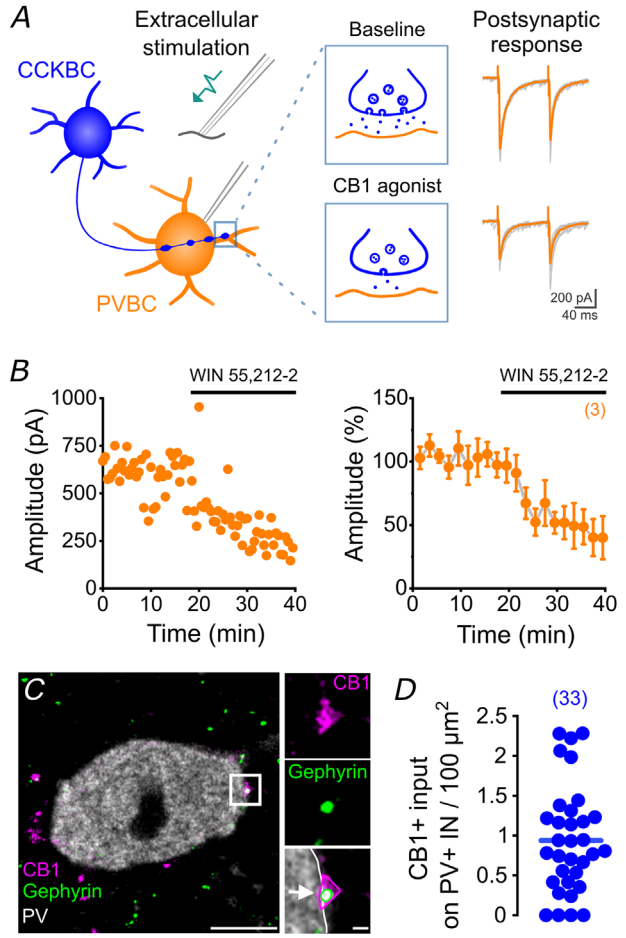

Figure 6. Pharmacological experiments and immunolabeling demonstrate the presence of functional CB1-positive inhibitory inputs received by PVBCs
A, schematic illustration of the experiment (left). Excitatory currents were blocked by 2 mM kynurenic acid in the recording solution. Representative traces of evoked IPSCs before (right, top) and after the application of CB1 agonist (right, bottom). Ten consecutive traces in grey, average in colour. *B*, inhibitory postsynaptic currents in a PVBC evoked by focal electrical stimulation are reduced by bath application of CB1 agonist WIN 55,212-2 (1 µM). Data from a representative experiment (left) and normalized data from $n = 3$ cells (right) from $n = 3$ BAC-PV-eGFP mice. Data points represent the mean ± SEM of four consecutive responses with an interstimulus interval of 30 s. *C*, confocal image of the soma of a PV+ interneuron labelled with immunostaining against PV. Inset: a terminal apposed to gephyrin labelling on the soma is immunopositive for CB1. Scale bars = 5 and 0.5 µm. *D*, quantification of the density of CB1+ terminals on PV-immunopositive somata ($n = 33$) from $n = 3$ C57Bl6 mice.

BCs have long been proposed to serve distinct circuit functions based on several differences in their single-cell features (Freund & Katona 2007). Our results regarding the contrasting input resistance, membrane time constant and accommodation ratio are in line with previous findings obtained in the hippocampus (Cea-del Rio et al., 2010; Glickfeld & Scanziani 2006; Lee et al., 2011; Pawelzik et al., 2002; Szabo et al., 2010), basal amygdala (Andrasi et al., 2017; Barsy et al., 2017) and neocortex (De-May

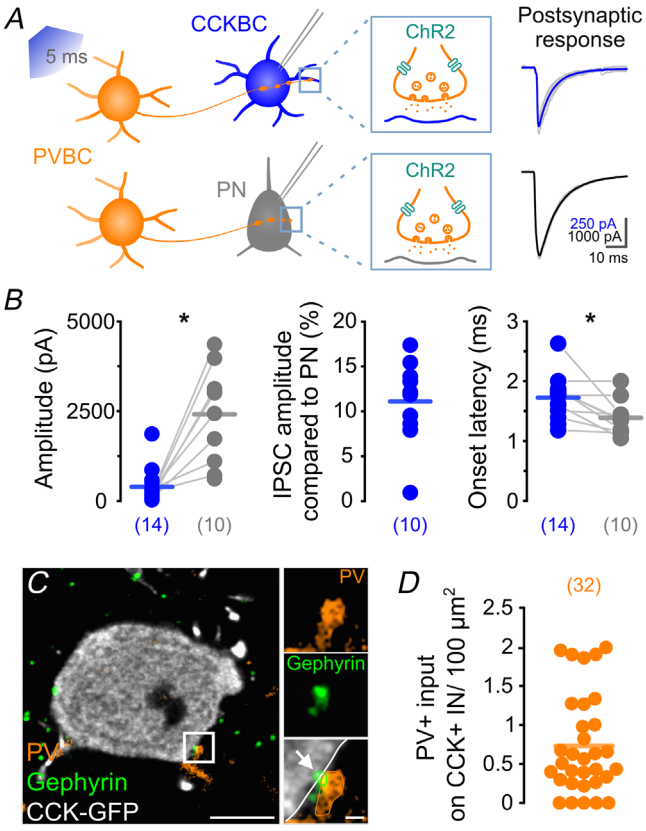

Figure 7. Postsynaptic responses upon light activation of PV+ cells via ChR2 together with anatomical data demonstrate that PVBCs innervate CCKBCs
A, schematic illustration of the experiment. Representative traces of light-evoked responses recorded simultaneously in a CCKBC (right, top) and a PN (right, bottom). Ten consecutive traces in grey, average in colour. *B*, features of the light-evoked postsynaptic responses. Data points representing simultaneously obtained recordings are connected on the graph from $n = 3$ Pvalb-IRES-Cre::BAC-CCK-DsRed mice. Numbers in parentheses represent the number of analyzed recordings. Mean amplitude of IPSCs recorded in CCKBCs and PNs (left, M–W, $P < 0.001$). Mean IPSC amplitude recorded in CCKBCs compared to the mean amplitude of IPSCs simultaneously recorded in PNs (middle). Onset latency of IPSCs (right, M–W, $P = 0.02062$). *C*, confocal image of the soma of a GFP-labelled CCK+ IN in the PrL of a VGAT-IRES-Cre::BAC-CCK-GFPcoIN mouse. Inset: a terminal immunopositive for PV apposed to gephyrin labelling, indicating the presence of an inhibitory synapse. Scale bars = 5 and 0.5 µm. *D*, quantification of the density of PV+ terminals on CCK+ interneurons ($n = 32$) in $n = 4$ VGAT-IRES-Cre::BAC-CCK-GFPcoIN mice.

& Ali 2013; Koukouli et al., 2022; Miyamae et al., 2017). These data provide further support to the concept that BCs are built to perform different tasks within cortical networks, despite targeting the same cellular domain in the PrL (Nagy-Pal et al., 2023). Notably, CCKBCs investigated here and in our previous study where we reported their morphological features (Nagy-Pal et al., 2023) probably correspond to previously described large CCK basket cells. In our dataset, no evidence was found for the presence of small CCK basket cells in the mouse PrL, an interneuron type that has been described in earlier studies (Karube et al., 2004; Kisvarday et al., 1985; Tremblay et al., 2016; Wang et al., 2002). If small CCK basket cells do not express CB1 at their axon terminals, then they may be very sparse in the mPFC because ∼90% of all GABAergic boutons that contacted the PN somata in the PrL were found to be immunopositive for CB1 or PV (Nagy-Pal et al., 2023).

By performing paired recordings, we showed that excitatory connections from local PNs give rise to significantly larger unitary currents in PVBCs compared to CCKBCs, in line with results obtained in the basal amygdala (Andrasi et al., 2017). Unitary EPSCs in PVBCs followed presynaptic spiking with shorter latency than in CCKBCs, which implies a general preference for the fast and precise activation of PVBCs over the recruitment of the CCKBC populations (Glickfeld & Scanziani 2006). On the other hand, we found that transmitter release after PN activation was similarly reliable from synapses contacting either type of BCs, which is in contrast to results showing higher ratio of failure at synapses contacting CCKBCs in the basal amygdala (Andrasi et al., 2017). Given the larger input resistance of CCKBCs compared to PVBCs (Fig. 1), increased transmission probability could be a way of recruiting CCKBCs more efficiently in the PrL compared to the basal amygdala. On the other hand, uEPSC on CCKBCs showed pronounced short-term depression compared to the steady uEPSCs recorded from PVBCs, a difference implying that sustained PN firing prefers to recruit PVBCs rather than CCKBCs. Although previous studies suggested that the synaptic transmission between PNs and PVBCs is strongly depressing, with a paired pulse ratio (PPR) of ∼0.6 in the hippocampus (Ali et al., 1998; Pouille & Scanziani 2004) and 0.7 in the neocortex (Reyes et al., 1998), recent investigations reported less pronounced depression at these synapses, with a PPR of 0.85 and 0.92 in the hippocampus (Aldahabi et al., 2022; Karlocai et al., 2021) and 0.89 in the basal amygdala (T. Andrasi & N. Hajos, unpublished observations). Thus, PPR of 1.06 observed in PN-PVBC pairs in the PrL are in line with the latest results.

Differences in the kinetics of uEPSCs were recapitulated in the rise time and decay kinetics of mEPSCs recorded in BCs. The slower rise time of miniature events in CCKBCs may suggest that excitatory synapses on this cell type are electrotonically more distant from the soma than those on PVBCs. Indeed, PVBCs receive many excitatory synaptic contacts on their somata (Gulyas et al., 1999; Hioki et al., 2013; Rovira-Esteban et al., 2020), in contrast to CCKBCs (Mátyás et al., 2004). However, it should be noted that, in the basal amygdala, uEPSCs in PVBCs and CCKBCs have been shown to exhibit different rise time kinetics despite the distance between the soma and the actual synaptic contacts being similar (Andrasi et al., 2017). The contrasting decay kinetics on the other hand might be explained, at least partially, by the AMPA receptor subunit composition on PVBCs because these cells were shown to express glutamate receptor subunit 4, which dictates rapid decay kinetics for EPSCs (Fuchs et al., 2007).

PVBC output synapses have long been regarded as reliable, fast transmitting sites of communication (Bartos et al., 2002; Buhl et al., 1995; Galarreta et al., 2008; Glickfeld & Scanziani 2006; Gonzalez-Burgos et al., 2005; Hefft & Jonas 2005; Maccaferri et al., 2000; Tamas et al.,

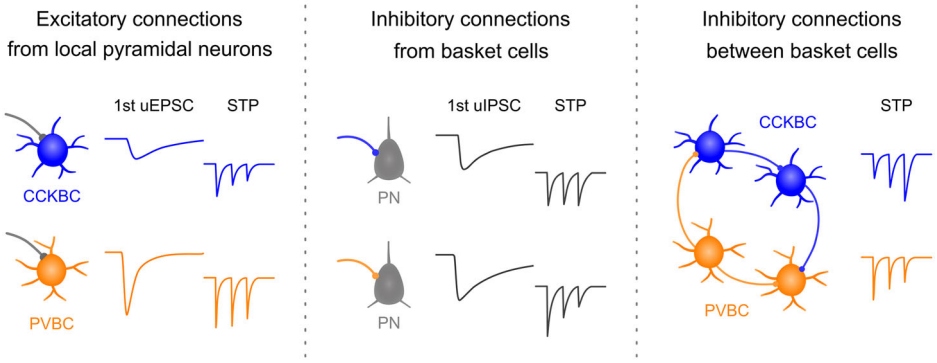

Figure 8. Key differences between synapses established within the microcircuits of the PrL
Summary of the key differences between synapses established by PNs and the two BC types within the microcircuits of the PrL. CCKBC, cholecystokinin-containing basket cell; PN, principal neuron; PVBC, parvalbumin-containing basket cell; STP, short-term plasticity; uEPSC, unitary excitatory postsynaptic current; uIPSC, unitary inhibitory post-synaptic current.

1997), and are features that we observed in the mouse PrL as well. The first uIPSCs evoked by PVBC spikes were followed by the strong depression in amplitude, as it is typical for synapses with high release probabilities (Zucker & Regehr 2002). By contrast, CCKBCs were able to maintain a steady level of inhibition during the time window of our action potential trains, although the amplitude of these uIPSCs remained small. Our observation that decay kinetics of the BC-evoked unitary currents in PNs are comparable is in line with previous reports (Andrasi et al., 2017; Barsy et al., 2017; Galarreta et al., 2008; Hefft & Jonas 2005; Kohus et al., 2016; Szabo et al., 2010; Veres et al., 2017), as well as the finding that hippocampal $GABA_A$ receptor subunit compositions are similar in synapses on PNs facing CCKBC or PVBC axon terminals (Kerti-Szigeti & Nusser 2016). However, the smaller variance in decay kinetics of PVBC synapses could be a necessary feature during rhythm generation (Buzsaki & Wang 2012) becuase changes in IPSC decay kinetics were shown to also impact the frequency of neuronal oscillations (Fisahn et al., 1998; Heistek et al., 2010; Pietersen et al., 2014). Apart from the similarities in uIPSC kinetics, BC output synapses are characterized by contrasting strength, precision and reliability in the mPFC as well.

Electrical coupling and chemical synapses between inhibitory cells can serve as means of enhancing synchronous activity (Bennett & Zukin 2004; Gibson et al., 1999; Tamas et al., 2000), comprising a circuit motif also utilized by PVBCs to aid rhythm generation in local circuits (Bartos et al., 2002; Beierlein et al., 2000). Studies show that inhibitory cells of the same class are frequently coupled (Andrasi et al., 2017; Galarreta et al., 2008; Meyer et al., 2002; Szabadics et al., 2001; Tamas et al., 2000) and our recordings obtained from CCKBCs strengthen this general concept (Iball & Ali 2011). However, PVBCs were connected to a lesser extent via gap junctions than expected based on prior studies, even though the recorded cells were located within 100 μm and innervated each other with chemical synapses in 52% of the tests. A reason behind this contradiction could be that studies reporting high connectivity rates via electrical synapses were typically obtained in juvenile animals (Coulon & Landisman 2017), whereas the number and strength of gap junctions between PVBCs were shown to decrease with age (Meyer et al., 2002). Our gap junction tests with PVBCs were recorded in animals older than P65 (mean age of 76 days, $n = 4$ animals), which might account for the decreased probability in electrical coupling between PVBCs. However, it cannot be ruled out that the low ratio of electrical connections between the sampled PVBCs was partly a result of the considerable distance between the gap junctions and the location of the recording pipettes because these connections were shown to occur up to several hundred μm away from the somata (Fukuda et al., 2006). Chemical synapses on the other hand displayed similar tendencies in terms of their strength, reliability and latency as the synapses that contact PNs, and as in homotypic paired recordings obtained in the hippocampus, where CCKBCs establish facilitating synapses but PVBC connections show synaptic depression (Bartos et al., 2001; Daw et al., 2009; Kohus et al., 2016). This facilitation at 40 Hz in synapses between CCKBCs appears to be stronger than in CCKBC synapses contacting PNs in both the mPFC and the hippocampus (Kohus et al., 2016).

Synaptic communication between the two BC types have only been investigated previously in a small number of studies (Andrasi et al., 2017; Dudok et al., 2021; Karson et al., 2009), despite the fact that inhibitory regulation is a major factor in the activity of interneurons as well, and, consequently, in the activity of neuronal circuits (Chamberland & Topolnik 2012). According to the quantifications of immunolabeled terminals in the primary somatosensory cortex, CCKBCs indeed establish synaptic connections with PV+ cells by providing 12% of the inhibitory boutons contacting PV+ somata (Hioki et al., 2018). Moreover, paired recordings obtained in the hippocampus reported functional synapses between the two types of BCs originating from CCKBCs (Karson et al., 2009) or PVBCs (Kohus et al., 2016). On the other hand, the same method led to the conclusion that the two BC types avoid innervating each other in the basal amygdala (Andrasi et al., 2017). Our pharmacological and optogenetic approaches combined with immunocytochemical investigations provided higher throughput than dual whole-cell recordings and were able to reveal connections between BC types in the mPFC, providing a further step towards deciphering BC operation.

Our results determining the characteristics of synaptic transmission and connectivity patterns of BCs help to refine our understanding about the building blocks of circuit operation in the PrL. Deeper knowledge of connectivity in prefrontal microcircuits in healthy brain is crucial to identify potential changes when these neuronal networks operate pathologically, which typifies many psychiatric disorders, including schizophrenia, attention deficit and autism. Revealing the deviations in circuit parameters in BC networks caused by genetic and/or environmental factors may help recognizing potential targets for interventional strategies, aiming to reduce often devastating symptoms.

References

Ahrlund-Richter, S., Xuan, Y., van Lunteren, J. A., Kim, H., Ortiz, C., Pollak Dorocic, I., Meletis, K., & Carlen, M. (2019). A whole-brain atlas of monosynaptic input targeting four different cell types in the medial prefrontal cortex of the mouse. *Nature Neuroscience*, **22**(4), 657–668.

Aldahabi, M., Balint, F., Holderith, N., Lorincz, A., Reva, M., & Nusser, Z. (2022). Different priming states of synaptic vesicles underlie distinct release probabilities at hippocampal excitatory synapses. *Neuron*, **110**(24), 4144–4161.e4147.

Ali, A. B., Deuchars, J., Pawelzik, H., & Thomson, A. M. (1998). CA1 pyramidal to basket and bistratified cell EPSPs: Dual intracellular recordings in rat hippocampal slices. *The Journal of Physiology*, **507(Pt 1)**(Pt 1), 201–217.

Andrasi, T., Veres, J. M., Rovira-Esteban, L., Kozma, R., Vikor, A., Gregori, E., & Hajos, N. (2017). Differential excitatory control of 2 parallel basket cell networks in amygdala microcircuits. *PLoS Biology*, **15**(5), e2001421.

Armstrong, C., & Soltesz, I. (2012). Basket cell dichotomy in microcircuit function. *The Journal of Physiology*, **590**(4), 683–694.

Atallah, B. V., Bruns, W., Carandini, M., & Scanziani, M. (2012). Parvalbumin-expressing interneurons linearly transform cortical responses to visual stimuli. *Neuron*, **73**(1), 159–170.

Barsy, B., Szabo, G. G., Andrasi, T., Vikor, A., & Hajos, N. (2017). Different output properties of perisomatic region-targeting interneurons in the basal amygdala. *European Journal of Neuroscience*, **45**(4), 548–558.

Bartos, M., Vida, I., Frotscher, M., Geiger, J. R., & Jonas, P. (2001). Rapid signaling at inhibitory synapses in a dentate gyrus interneuron network. *Journal of Neuroscience*, **21**(8), 2687–2698.

Bartos, M., Vida, I., Frotscher, M., Meyer, A., Monyer, H., Geiger, J. R., & Jonas, P. (2002). Fast synaptic inhibition promotes synchronized gamma oscillations in hippocampal interneuron networks. *Proceedings of the National Academy of Sciences of the United States of America*, **99**(20), 13222–13227.

Beierlein, M., Gibson, J. R., & Connors, B. W. (2000). A network of electrically coupled interneurons drives synchronized inhibition in neocortex. *Nature Neuroscience*, **3**(9), 904–910.

Bennett, M. V., & Zukin, R. S. (2004). Electrical coupling and neuronal synchronization in the Mammalian brain. *Neuron*, **41**(4), 495–511.

Bienvenu, T. C., Busti, D., Magill, P. J., Ferraguti, F., & Capogna, M. (2012). Cell-type-specific recruitment of amygdala interneurons to hippocampal theta rhythm and noxious stimuli in vivo. *Neuron*, **74**(6), 1059–1074.

Bodor, A. L., Katona, I., Nyiri, G., Mackie, K., Ledent, C., Hajos, N., & Freund, T. F. (2005). Endocannabinoid signaling in rat somatosensory cortex: Laminar differences and involvement of specific interneuron types. *Journal of Neuroscience*, **25**(29), 6845–6856.

Buhl, E. H., Cobb, S. R., Halasy, K., & Somogyi, P. (1995). Properties of unitary IPSPs evoked by anatomically identified basket cells in the rat hippocampus. *European Journal of Neuroscience*, **7**(9), 1989–2004.

Buzsaki, G., & Wang, X. J. (2012). Mechanisms of gamma oscillations. *Annual Review of Neuroscience*, **35**, 203–225.

Cardin, J. A., Carlen, M., Meletis, K., Knoblich, U., Zhang, F., Deisseroth, K., Tsai, L. H., & Moore, C. I. (2009). Driving fast-spiking cells induces gamma rhythm and controls sensory responses. *Nature*, **459**(7247), 663–667.

Cea-del Rio, C. A., Lawrence, J. J., Tricoire, L., Erdelyi, F., Szabo, G., & McBain, C. J. (2010). M3 muscarinic acetylcholine receptor expression confers differential cholinergic modulation to neurochemically distinct hippocampal basket cell subtypes. *Journal of Neuroscience*, **30**(17), 6011–6024.

Chamberland, S., & Topolnik, L. (2012). Inhibitory control of hippocampal inhibitory neurons. *Frontiers in Neuroscience*, **6**, 165.

Cobb, S. R., Buhl, E. H., Halasy, K., Paulsen, O., & Somogyi, P. (1995). Synchronization of neuronal activity in hippocampus by individual GABAergic interneurons. *Nature*, **378**(6552), 75–78.

Coulon, P., & Landisman, C. E. (2017). The potential role of gap junctional plasticity in the regulation of state. *Neuron*, **93**(6), 1275–1295.

Daw, M. I., Tricoire, L., Erdelyi, F., Szabo, G., & McBain, C. J. (2009). Asynchronous transmitter release from cholecystokinin-containing inhibitory interneurons is widespread and target-cell independent. *Journal of Neuroscience*, **29**(36), 11112–11122.

De-May, C. L., & Ali, A. B. (2013). Cell type-specific regulation of inhibition via cannabinoid type 1 receptors in rat neocortex. *Journal of Neurophysiology*, **109**(1), 216–224.

Dudok, B., Klein, P. M., Hwaun, E., Lee, B. R., Yao, Z., Fong, O., Bowler, J. C., Terada, S., Sparks, F. T., Szabo, G. G., Farrell, J. S., Berg, J., Daigle, T. L., Tasic, B., Dimidschstein, J., Fishell, G., Losonczy, A., Zeng, H., & Soltesz, I. (2021). Alternating sources of perisomatic inhibition during behavior. *Neuron*, **109**(6), 997–1012. e1019.

Fisahn, A., Pike, F. G., Buhl, E. H., & Paulsen, O. (1998). Cholinergic induction of network oscillations at 40 Hz in the hippocampus in vitro. *Nature*, **394**(6689), 186–189.

Freund, T. F., & Katona, I. (2007). Perisomatic inhibition. *Neuron*, **56**(1), 33–42.

Fuchs, E. C., Zivkovic, A. R., Cunningham, M. O., Middleton, S., Lebeau, F. E., Bannerman, D. M., Rozov, A., Whittington, M. A., Traub, R. D., Rawlins, J. N., & Monyer, H. (2007). Recruitment of parvalbumin-positive interneurons determines hippocampal function and associated behavior. *Neuron*, **53**(4), 591–604.

Fukuda, T., Kosaka, T., Singer, W., & Galuske, R. A. (2006). Gap junctions among dendrites of cortical GABAergic neurons establish a dense and widespread intercolumnar network. *Journal of Neuroscience*, **26**(13), 3434–3443.

Galarreta, M., Erdelyi, F., Szabo, G., & Hestrin, S. (2008). Cannabinoid sensitivity and synaptic properties of 2 GABAergic networks in the neocortex. *Cerebral Cortex*, **18**(10), 2296–2305.

Galarreta, M., & Hestrin, S. (1998). Frequency-dependent synaptic depression and the balance of excitation and inhibition in the neocortex. *Nature Neuroscience*, **1**(7), 587–594.

Galarreta, M., & Hestrin, S. (1999). A network of fast-spiking cells in the neocortex connected by electrical synapses. *Nature*, **402**(6757), 72–75.

Gibson, J. R., Beierlein, M., & Connors, B. W. (1999). Two networks of electrically coupled inhibitory neurons in neocortex. *Nature*, **402**(6757), 75–79.

Glausier, J. R., Fish, K. N., & Lewis, D. A. (2014). Altered parvalbumin basket cell inputs in the dorsolateral prefrontal cortex of schizophrenia subjects. *Molecular Psychiatry*, **19**(1), 30–36.

Glickfeld, L. L., & Scanziani, M. (2006). Distinct timing in the activity of cannabinoid-sensitive and cannabinoid-insensitive basket cells. *Nature Neuroscience*, **9**(6), 807–815.

Gonzalez-Burgos, G., Cho, R. Y., & Lewis, D. A. (2015). Alterations in cortical network oscillations and parvalbumin neurons in schizophrenia. *Biological Psychiatry*, **77**(12), 1031–1040.

Gonzalez-Burgos, G., Krimer, L. S., Povysheva, N. V., Barrionuevo, G., & Lewis, D. A. (2005). Functional properties of fast spiking interneurons and their synaptic connections with pyramidal cells in primate dorsolateral prefrontal cortex. *Journal of Neurophysiology*, **93**(2), 942–953.

Grundy, D. (2015). Principles and standards for reporting animal experiments in The Journal of Physiology and Experimental Physiology. *The Journal of Physiology*, **593**(12), 2547–2549.

Gulyas, A. I., Megias, M., Emri, Z., & Freund, T. F. (1999). Total number and ratio of excitatory and inhibitory synapses converging onto single interneurons of different types in the CA1 area of the rat hippocampus. *Journal of Neuroscience*, **19**(22), 10082–10097.

Gulyas, A. I., Miles, R., Hajos, N., & Freund, T. F. (1993). Precision and variability in postsynaptic target selection of inhibitory cells in the hippocampal CA3 region. *European Journal of Neuroscience*, **5**(12), 1729–1751.

Gulyas, A. I., Szabo, G. G., Ulbert, I., Holderith, N., Monyer, H., Erdelyi, F., Szabo, G., Freund, T. F., & Hajos, N. (2010). Parvalbumin-containing fast-spiking basket cells generate the field potential oscillations induced by cholinergic receptor activation in the hippocampus. *Journal of Neuroscience*, **30**(45), 15134–15145.

Hafner, G., Witte, M., Guy, J., Subhashini, N., Fenno, L. E., Ramakrishnan, C., Kim, Y. S., Deisseroth, K., Callaway, E. M., Oberhuber, M., Conzelmann, K. K., & Staiger, J. F. (2019). Mapping brain-wide afferent inputs of parvalbumin-expressing GABAergic neurons in barrel cortex reveals local and long-range circuit motifs. *Cell Reports*, **28**(13), 3450–3461. e3458.

Hajos, N., Katona, I., Naiem, S. S., MacKie, K., Ledent, C., Mody, I., & Freund, T. F. (2000). Cannabinoids inhibit hippocampal GABAergic transmission and network oscillations. *European Journal of Neuroscience*, **12**(9), 3239–3249.

Halasy, K., Buhl, E. H., Lorinczi, Z., Tamas, G., & Somogyi, P. (1996). Synaptic target selectivity and input of GABAergic basket and bistratified interneurons in the CA1 area of the rat hippocampus. *Hippocampus*, **6**(3), 306–329.

Hashimoto, T., Volk, D. W., Eggan, S. M., Mirnics, K., Pierri, J. N., Sun, Z., Sampson, A. R., & Lewis, D. A. (2003). Gene expression deficits in a subclass of GABA neurons in the prefrontal cortex of subjects with schizophrenia. *Journal of Neuroscience*, **23**(15), 6315–6326.

Hefft, S., & Jonas, P. (2005). Asynchronous GABA release generates long-lasting inhibition at a hippocampal interneuron-principal neuron synapse. *Nature Neuroscience*, **8**(10), 1319–1328.

Heistek, T. S., Jaap Timmerman, A., Spijker, S., Brussaard, A. B., & Mansvelder, H. D. (2010). GABAergic synapse properties may explain genetic variation in hippocampal network oscillations in mice. *Frontiers in Cellular Neuroscience*, **4**, 18.

Hijazi, S., Smit, A. B., & van Kesteren, R. E. (2023). Fast-spiking parvalbumin-positive interneurons in brain physiology and Alzheimer's disease. *Molecular Psychiatry*, **28**(12), 4954–4967.

Hioki, H., Okamoto, S., Konno, M., Kameda, H., Sohn, J., Kuramoto, E., Fujiyama, F., & Kaneko, T. (2013). Cell type-specific inhibitory inputs to dendritic and somatic compartments of parvalbumin-expressing neocortical interneuron. *Journal of Neuroscience*, **33**(2), 544–555.

Hioki, H., Sohn, J., Nakamura, H., Okamoto, S., Hwang, J., Ishida, Y., Takahashi, M., & Kameda, H. (2018). Preferential inputs from cholecystokinin-positive neurons to the somatic compartment of parvalbumin-expressing neurons in the mouse primary somatosensory cortex. *Brain Research*, **1695**, 18–30.

Hu, H., Gan, J., & Jonas, P. (2014). Interneurons. Fast-spiking, parvalbumin(+) GABAergic interneurons: From cellular design to microcircuit function. *Science*, **345**(6196), 1255263.

Hu, H., Roth, F. C., Vandael, D., & Jonas, P. (2018). Complementary tuning of Na(+) and K(+) channel gating underlies fast and energy-efficient action potentials in GABAergic interneuron axons. *Neuron*, **98**(1), 156–165. e156.

Iball, J., & Ali, A. B. (2011). Endocannabinoid release modulates electrical coupling between CCK cells connected via chemical and electrical synapses in CA1. *Frontiers in Neural Circuits*, **5**, 17.

Karlocai, M. R., Heredi, J., Benedek, T., Holderith, N., Lorincz, A., & Nusser, Z. (2021). Variability in the Munc13-1 content of excitatory release sites. *eLife*, **10**, e67468.

Karson, M. A., Tang, A. H., Milner, T. A., & Alger, B. E. (2009). Synaptic cross talk between perisomatic-targeting interneuron classes expressing cholecystokinin and parvalbumin in hippocampus. *Journal of Neuroscience*, **29**(13), 4140–4154.

Karube, F., Kubota, Y., & Kawaguchi, Y. (2004). Axon branching and synaptic bouton phenotypes in GABAergic nonpyramidal cell subtypes. *Journal of Neuroscience*, **24**(12), 2853–2865.

Katona, I., Rancz, E. A., Acsady, L., Ledent, C., Mackie, K., Hajos, N., & Freund, T. F. (2001). Distribution of CB1 cannabinoid receptors in the amygdala and their role in the control of GABAergic transmission. *Journal of Neuroscience*, **21**(23), 9506–9518.

Katona, I., Sperlagh, B., Sik, A., Kafalvi, A., Vizi, E. S., Mackie, K., & Freund, T. F. (1999). Presynaptically located CB1 cannabinoid receptors regulate GABA release from axon terminals of specific hippocampal interneurons. *Journal of Neuroscience*, **19**(11), 4544–4558.

Kawaguchi, Y., & Kubota, Y. (1998). Neurochemical features and synaptic connections of large physiologically-identified GABAergic cells in the rat frontal cortex. *Neuroscience*, **85**(3), 677–701.

Kawaguchi, Y., & Shindou, T. (1998). Noradrenergic excitation and inhibition of GABAergic cell types in rat frontal cortex. *Journal of Neuroscience*, **18**(17), 6963–6976.

Kerti-Szigeti, K., & Nusser, Z. (2016). Similar GABAA receptor subunit composition in somatic and axon initial segment synapses of hippocampal pyramidal cells. *eLife*, **5**, e18426.

Kim, D., Jeong, H., Lee, J., Ghim, J. W., Her, E. S., Lee, S. H., & Jung, M. W. (2016). Distinct roles of parvalbumin- and somatostatin-expressing interneurons in working memory. *Neuron*, **92**(4), 902–915.

Kisvarday, Z. F., Martin, K. A., Whitteridge, D., & Somogyi, P. (1985). Synaptic connections of intracellularly filled clutch cells: A type of small basket cell in the visual cortex of the cat. *Journal of Comparative Neurology*, **241**(2), 111–137.

Kohus, Z., Kali, S., Rovira-Esteban, L., Schlingloff, D., Papp, O., Freund, T. F., Hajos, N., & Gulyas, A. I. (2016). Properties and dynamics of inhibitory synaptic communication within the CA3 microcircuits of pyramidal cells and interneurons expressing parvalbumin or cholecystokinin. *The Journal of Physiology*, **594**(13), 3745–3774.

Koukouli, F., Montmerle, M., Aguirre, A., De Brito Van Velze, M., Peixoto, J., Choudhary, V., Varilh, M., Julio-Kalajzic, F., Allene, C., Mendez, P., Zerlaut, Y., Marsicano, G., Schluter, O. M., Rebola, N., Bacci, A., & Lourenco, J. (2022). Visual-area-specific tonic modulation of GABA release by endocannabinoids sets the activity and coordination of neocortical principal neurons. *Cell reports*, **40**(8), 111202.

Kubota, Y., Kondo, S., Nomura, M., Hatada, S., Yamaguchi, N., Mohamed, A. A., Karube, F., Lubke, J., & Kawaguchi, Y. (2015). Functional effects of distinct innervation styles of pyramidal cells by fast spiking cortical interneurons. *eLife*, **4**, e07919.

Lagler, M., Ozdemir, A. T., Lagoun, S., Malagon-Vina, H., Borhegyi, Z., Hauer, R., Jelem, A., & Klausberger, T. (2016). Divisions of identified parvalbumin-expressing basket cells during working memory-guided decision making. *Neuron*, **91**(6), 1390–1401.

Lee, S. Y., Foldy, C., Szabadics, J., & Soltesz, I. (2011). Cell-type-specific CCK2 receptor signaling underlies the cholecystokinin-mediated selective excitation of hippocampal parvalbumin-positive fast-spiking basket cells. *Journal of Neuroscience*, **31**(30), 10993–11002.

Lu, J., Tucciarone, J., Padilla-Coreano, N., He, M., Gordon, J. A., & Huang, Z. J. (2017). Selective inhibitory control of pyramidal neuron ensembles and cortical subnetworks by chandelier cells. *Nature Neuroscience*, **20**(10), 1377–1383.

Maccaferri, G., Roberts, J. D., Szucs, P., Cottingham, C. A., & Somogyi, P. (2000). Cell surface domain specific post-synaptic currents evoked by identified GABAergic neurones in rat hippocampus in vitro. *The Journal of Physiology*, **524 Pt 1**(Pt 1), 91–116.

Mate, Z., Poles, M. Z., Szabo, G., Bagyanszki, M., Talapka, P., Fekete, E., & Bodi, N. (2013). Spatiotemporal expression pattern of DsRedT3/CCK gene construct during postnatal development of myenteric plexus in transgenic mice. *Cell and Tissue Research*, **352**(2), 199–206.

Mátyás, F., Freund, T. F., & Gulyás, A. I. (2004). Convergence of excitatory and inhibitory inputs onto CCK-containing basket cells in the CA1 area of the rat hippocampus. *European Journal of Neuroscience*, **19**(5), 1243–1256.

Meyer, A. H., Katona, I., Blatow, M., Rozov, A., & Monyer, H. (2002). In vivo labeling of parvalbumin-positive interneurons and analysis of electrical coupling in identified neurons. *Journal of Neuroscience*, **22**(16), 7055–7064.

Miles, R., Toth, K., Gulyas, A. I., Hajos, N., & Freund, T. F. (1996). Differences between somatic and dendritic inhibition in the hippocampus. *Neuron*, **16**(4), 815–823.

Miyamae, T., Chen, K., Lewis, D. A., & Gonzalez-Burgos, G. (2017). Distinct physiological maturation of parvalbumin-positive neuron subtypes in mouse prefrontal cortex. *Journal of Neuroscience*, **37**(19), 4883–4902.

Nagy-Pal, P., Veres, J. M., Fekete, Z., Karlocai, M. R., Weisz, F., Barabas, B., Reeb, Z., & Hajos, N. (2023). Structural organisation of perisomatic inhibition in the mouse medial prefrontal cortex. *Journal of Neuroscience*, **43**(42), 6972–6987.

Pawelzik, H., Hughes, D. I., & Thomson, A. M. (2002). Physiological and morphological diversity of immunocytochemically defined parvalbumin- and cholecystokinin-positive interneurones in CA1 of the adult rat hippocampus. *Journal of Comparative Neurology*, **443**(4), 346–367.

Pfeffer, C. K., Xue, M., He, M., Huang, Z. J., & Scanziani, M. (2013). Inhibition of inhibition in visual cortex: The logic of connections between molecularly distinct interneurons. *Nature Neuroscience*, **16**(8), 1068–1076.

Pietersen, A. N., Ward, P. D., Hagger-Vaughan, N., Wiggins, J., Jefferys, J. G., & Vreugdenhil, M. (2014). Transition between fast and slow gamma modes in rat hippocampus area CA1 in vitro is modulated by slow CA3 gamma oscillations. *The Journal of Physiology*, **592**(4), 605–620.

Pouille, F., & Scanziani, M. (2004). Routing of spike series by dynamic circuits in the hippocampus. *Nature*, **429**(6993), 717–723.

Reyes, A., Lujan, R., Rozov, A., Burnashev, N., Somogyi, P., & Sakmann, B. (1998). Target-cell-specific facilitation and depression in neocortical circuits. *Nature Neuroscience*, **1**(4), 279–285.

Rovira-Esteban, L., Hajos, N., Nagy, G. A., Crespo, C., Nacher, J., Varea, E., & Blasco-Ibanez, J. M. (2020). Semilunar granule cells are the primary source of the perisomatic excitatory innervation onto parvalbumin-expressing interneurons in the dentate gyrus. *eNeuro*, **7**(4).

Rudy, B., & McBain, C. J. (2001). Kv3 channels: voltage-gated K+ channels designed for high-frequency repetitive firing. *Trends in Neuroscience (Tins)*, **24**(9), 517–526.

Sassoe-Pognetto, M., & Fritschy, J. M. (2000). Mini-review: Gephyrin, a major postsynaptic protein of GABAergic synapses. *European Journal of Neuroscience*, **12**(7), 2205–2210.

Schlingloff, D., Kali, S., Freund, T. F., Hajos, N., & Gulyas, A. I. (2014). Mechanisms of sharp wave initiation and ripple generation. *Journal of Neuroscience*, **34**(34), 11385–11398.
Shu, S., Xu, S. Y., Ye, L., Liu, Y., Cao, X., Jia, J. Q., Bian, H. J., Liu, Y., Zhu, X. L., & Xu, Y. (2023). Prefrontal parvalbumin interneurons deficits mediate early emotional dysfunction in Alzheimer's disease. *Neuropsychopharmacology*, **48**(2), 391–401.
Sohal, V. S., Zhang, F., Yizhar, O., & Deisseroth, K. (2009). Parvalbumin neurons and gamma rhythms enhance cortical circuit performance. *Nature*, **459**(7247), 698–702.
Somogyi, P., Kisvarday, Z. F., Martin, K. A., & Whitteridge, D. (1983). Synaptic connections of morphologically identified and physiologically characterized large basket cells in the striate cortex of cat. *Neuroscience*, **10**(2), 261–294.
Stark, E., Roux, L., Eichler, R., Senzai, Y., Royer, S., & Buzsaki, G. (2014). Pyramidal cell-interneuron interactions underlie hippocampal ripple oscillations. *Neuron*, **83**(2), 467–480.
Szabadics, J., Lorincz, A., & Tamas, G. (2001). Beta and gamma frequency synchronization by dendritic gabaergic synapses and gap junctions in a network of cortical interneurons. *Journal of Neuroscience*, **21**(15), 5824–5831.
Szabo, G. G., Holderith, N., Gulyas, A. I., Freund, T. F., & Hajos, N. (2010). Distinct synaptic properties of perisomatic inhibitory cell types and their different modulation by cholinergic receptor activation in the CA3 region of the mouse hippocampus. *European Journal of Neuroscience*, **31**(12), 2234–2246.
Tamas, G., Buhl, E. H., Lorincz, A., & Somogyi, P. (2000). Proximally targeted GABAergic synapses and gap junctions synchronize cortical interneurons. *Nature Neuroscience*, **3**(4), 366–371.
Tamas, G., Buhl, E. H., & Somogyi, P. (1997). Fast IPSPs elicited via multiple synaptic release sites by different types of GABAergic neurone in the cat visual cortex. *The Journal of Physiology*, **500**(Pt 3), 715–738.
Tremblay, R., Lee, S., & Rudy, B. (2016). GABAergic interneurons in the neocortex: From cellular properties to circuits. *Neuron*, **91**(2), 260–292.
Varga, C., Lee, S. Y., & Soltesz, I. (2010). Target-selective GABAergic control of entorhinal cortex output. *Nature Neuroscience*, **13**(7), 822–824.
Vereczki, V. K., Muller, K., Krizsan, E., Mate, Z., Fekete, Z., Rovira-Esteban, L., Veres, J. M., Erdelyi, F., & Hajos, N. (2021). Total number and ratio of GABAergic neuron types in the mouse lateral and basal amygdala. *Journal of Neuroscience*, **41**(21), 4575–4595.
Veres, J. M., Nagy, G. A., & Hajos, N. (2017). Perisomatic GABAergic synapses of basket cells effectively control principal neuron activity in amygdala networks. *eLife*, **6**, e20721.
Wang, Y., Gupta, A., Toledo-Rodriguez, M., Wu, C. Z., & Markram, H. (2002). Anatomical, physiological, molecular and circuit properties of nest basket cells in the developing somatosensory cortex. *Cerebral Cortex*, **12**(4), 395–410.
Wilson, R. I., Kunos, G., & Nicoll, R. A. (2001). Presynaptic specificity of endocannabinoid signaling in the hippocampus. *Neuron*, **31**(3), 453–462.
Wilson, R. I., & Nicoll, R. A. (2001). Endogenous cannabinoids mediate retrograde signalling at hippocampal synapses. *Nature*, **410**(6828), 588–592.
Woodruff, A. R., & Sah, P. (2007). Inhibition and synchronization of basal amygdala principal neuron spiking by parvalbumin-positive interneurons. *Journal of Neurophysiology*, **98**(5), 2956–2961.
Zucker, R. S., & Regehr, W. G. (2002). Short-term synaptic plasticity. *Annual Review of Physiology*, **64**, 355–405.

Additional information

Data availability statement

The data supporting the findings of the present study are available from the corresponding author upon reasonable request.

Competing interests

The authors declare no competing financial interests.

Author contributions

The experiments were conducted in the Laboratory of Network Neurophysiology at the HUN-REN Institute of Experimental Medicine. Z.F., F.W., M.R.K. and J.M.V. were responsible for acquisition. Z.F., F.W., M.R.K. and J.M.V. were responsible for analysis of data. Z.F., F.W., M.R.K., J.M.V. and T.A. were responsible for interpretation of data. Z.F. and N.H. were responsible for writing the manuscript. F.W., M.R.K., J.M.V. and T.A. were responsible for revising the work critically for important intellectual content. J.M.V. and N.H. were responsible for design of the work. All authors confirm that they approved the final version of the manuscript submitted for publication. All authors agree to be accountable for all aspects of the work in ensuring that questions related to the accuracy or integrity of any part of the work are appropriately investigated and resolved. All persons designated as authors qualify for authorship, and all those who qualify for authorship are listed.

Funding

Funding was received from the HUN-REN Hungarian Research Network, Hungarian Brain Research Program (2017-1.2.1-NKP-2017-00002) and National Research, Development and Innovation Office (K131893).

Acknowledgements

We are grateful to Éva Krizsán and Erzsébet Gregori for their excellent technical assistance. We also thank Pál Vági and László Barna, the Nikon Microscopy Centre at the Institute of Experimental Medicine, Nikon Austria GmbH, and Auro-Science Consulting, Ltd, for kindly providing microscopy support.

Keywords

excitatory synaptic transmission, GABAergic, inhibitory synaptic transmission, interneurons, prelimbic cortex

Supporting information

Additional supporting information can be found online in the Supporting Information section at the end of the HTML view of the article. Supporting information files available:

Peer Review History